INSTYTUT FIZYKI
POLSKIEJ AKADEMII NAUK
Institute of Physics, Polish Academy of Sciences

DOCTORAL THESIS

# Molecular Dynamics Simulation of the Coalescence of Freely Suspended and Sessile Droplets

*Author:*
Soheil ARBABI

*Supervisor:*
Dr hab. Panagiotis THEODORAKIS

*A thesis submitted in fulfillment of the requirements for the degree of Doctor of Philosophy* in Physics

Division of Theoretical Physics
Soft Matter and Fluids Physics Group

February 15, 2024

Abstract of thesis entitled

# Molecular Dynamics Simulation of the Coalescence of Freely Suspended and Sessile Droplets

Submitted by

**Soheil ARBABI**

for the degree of Doctor of Philosophy

at Institute of Physics, Polish Academy of Sciences

in February, 2024

The coalescence of droplets is an everyday natural process, wherein raindrops combine as they descend, forming larger raindrops. Alternatively, they may unite upon the surface of a leaf, crafting a picturesque dew on a crisp early autumn morning. Furthermore, this phenomenon has numerous applications. For instance, in inkjet printing, achieving high-quality prints depends on the flawless coalescence of color drops on the paper's surface. In microfluidics, encapsulating bio-particles within droplets become feasible by adding surfactants to hinder coalescence. Numerous studies have attempted to explain coalescence through numerical and experimental approaches. However, these methods often suffer from a lack of resolution, particularly in the initial stages of coalescence, known as the 'pinching stage'. This stage remains inaccessible in terms of both length and time scales in continuum and experimental studies. It is where molecular dynamics can play a role by offering extremely fine resolution in time and space to capture the initial pinching. Following pinching, the formation of a bridge between two droplets occurs. The growth dynamics of this bridge takes place within different regimes, and various controversial explanations have been proposed about these different regimes involved in this process. Furthermore, describing the mass transport mechanism of surfactant molecules during coalescence presents another challenge. In continuum simulations, researchers can investigate the convection and diffusion of surfactants as a result of capillary forces, primarily arising from the curved interface of the bridge between two droplets. Additionally, Marangoni effects come into play, generating surface flows due to surface tension gradients in the presence of surfactants. The mathematical description of these processes involves various equations, each based on specific assumptions. However, a knowledge gap persists in the detailed description of surfactant mass transport with molecular resolution, particularly concerning the bridge and the initial stages of coalescence. In the case of coalescence of sessile droplets, much less is known, despite its relevance for microfluidics and coating technologies. Different types of substrate ranging from non-wettable to wettable substrate can affect the coalescence process and bridge growth dynamics.

The objective of this thesis is to offer a comprehensive explanation of droplet coalescence by utilizing the Molecular Dynamics method. This investigation encompasses three distinct types of surfactants and various concentrations. Additionally, polymer droplets with different chain lengths are taken into consideration. The presence of two distinct regimes within the dynamics of bridge growth has been observed in this study: the Thermal and Inertial regimes. Notably, it has been demonstrated that the transition between these two regimes becomes more pronounced when the surfactant concentration is well above the Critical Aggregation Concentration (CAC). Furthermore, a second objective of this thesis is to provide a comprehensive explanation of the mass transport mechanism. Here, the mass transport mechanism during coalescence is compared and investigated for surfactant concentrations both below and above the CAC, considering three different surfactants. The findings reveal that the coalescence process is initiated by surfactant pinching, followed by the formation of a surfactant film between the two droplets. In cases where the concentration exceeds the CAC, this film becomes continuous, thereby hindering the participation of water in the initial stages of coalescence. Moreover, large-scale molecular dynamics simulations are utilized to investigate the coalescence of surfactant-laden sessile droplets on substrates with varying wettability. Noteworthy, similarities are observed between the coalescence of sessile droplets with equilibrium contact angles exceeding $90^\circ$ and that of freely suspended droplets. A significant shift in bridge dynamics and the mass transport mechanism becomes apparent below the $90^\circ$ contact angle, where the initial contact point transforms into a small, line-like structure, exerting a pronounced influence on various aspects of the coalescence process. This configuration allows water to actively participate in the coalescence from the outset. Finally, the coalescence of sessile polymer droplets with different chain lengths is studied, considering the effects of substrate wettability and droplet viscosity on coalescence and bridge growth dynamics. The study reveals that the presence of the substrate and its wettability significantly influence bridge dynamics. In general, increasing the polymer chain length results in a reduction in the bridge growth rate and coalescence speed.

Thus, we anticipate that the present thesis provides a comprehensive account of droplet coalescence, which can play an important role in various applications requiring a detailed understanding of droplet coalescence behavior. This pertains to both freely suspended and sessile droplets, making it of primary interest. Additionally, this study has the potential to create new opportunities, such as advances in droplet research. For instance, it can offer innovative solutions in cases where both numerical and experimental methods face challenges in capturing minute scales, be it at the nano, micro, or smaller levels.

Streszczenie pracy doktorskiej pt

**Symulacja dynamiki molekularnej koalescencji swobodnie zawieszone i siedzące kropelki**

Instytut Fizyki PAN

Przesłane przez

**Soheil ARBABI**

Koalescencja kropelek jest codziennym, naturalnym procesem, podczas którego krople deszczu łączą się podczas opadania, tworząc większe krople deszczu. Alternatywnie mogą zjednoczyć się na powierzchni liścia, tworząc malowniczą rosę w rześki wczesny jesienny poranek. Co więcej, zjawisko to znajduje liczne zastosowania. Na przykład w druku atramentowym uzyskanie wysokiej jakości wydruków zależy od precyzyjnej koalescencji kropel farby na powierzchni papieru. W mikrofluidyce kapsułkowanie biocząstek w kropelkach staje się możliwe poprzez dodanie surfaktantów utrudniających koalescencję. W licznych badaniach próbowano wyjaśnić koalescencję zarówno metodami numerycznymi, jak i eksperymentalnymi. Jednakże metody te często charakteryzują się słabą rozdzielczością, szczególnie w początkowym stadium koalescencji, znanym jako „etap szczypnięcia". Etap ten pozostaje niedostępny zarówno pod względem rozdzielczości przestrzennych i czasowych, w symulacjach metodą kontinuum i eksperymentalnych. To właśnie tu rolę może odegrać dynamika molekularna, która zapewnia odpowiednio wysoką rozdzielczość w czasie i przestrzeni, aby uchwycić początkową fazę szczypnięcia. Po szczypnięciu następuje utworzenie mostu pomiędzy dwiema kropelkami. Dynamika wzrostu tego pomostu odbywa się w ramach różnych reżimów; zaproponowano dotychczas różne sporne wyjaśnienia dotyczące tego zjawiska. Ponadto opisanie mechanizmu transportu masy cząsteczek surfaktantu podczas koalescencji stanowi kolejne wyzwanie. W symulacjach ciągłych możliwe jest zbadanie konwekcji i dyfuzji surfaktantów pod wpływem sił kapilarnych, wynikających głównie z zakrzywionej powierzchni styku między dwiema kropelkami. Dodatkowo w grę wchodzą efekty Marangoniego, generujące przepływy powierzchniowe w wyniku gradientów napięcia powierzchniowego w obecności surfaktantu. Matematyczny opis tych procesów obejmuje różne równania, każde oparte na określonych założeniach.

Jednakże niejasne pozostają szczegóły opisu transportu masy surfaktantów w skali molekularnej, szczególnie w odniesieniu do pomostu i początkowych etapów koalescencji. W przypadku koalescencji kropelek osiadłych wiadomo jeszcze znacznie mniej, pomimo znaczenia tego przypadku dla mikroprzepływów i technologii powlekania. Różne rodzaje podłoża, od niezwilżalnego do zwilżalnego, mogą wpływać na proces koalescencji i dynamikę wzrostu mostka.

Celem tej pracy jest kompleksowe wyjaśnienie koalescencji kropel z wykorzystaniem metod dynamiki molekularnej. Badanie to obejmuje trzy różne typy surfaktantów i różne stężenia. Dodatkowo brane są pod uwagę kropelki polimerów o różnych długościach łańcucha. W niniejszej pracy zaobserwowano obecność dwóch odrębnych reżimów w dynamice wzrostu mostów: reżim termiczny i inercyjny. W szczególności wykazano, że przejście między tymi dwoma reżimami staje się bardziej wyraźne, gdy stężenie surfaktantu znacznie przekracza CAC (krytyczne stężenie agregacji). Ponadto drugim celem tej pracy jest kompleksowe wyjaśnienie mechanizmu transportu masowego. Tutaj porównany zostaje mechanizm transportu masy podczas koalescencji pod kątem stężeń surfaktantu zarówno poniżej, jak i powyżej CAC, obejmując trzy różne gatunki surfaktantu. Wyniki pokazują, że proces koalescencji rozpoczyna się od lokalnego wzrostu koncentracji surfaktantu, po czym następuje utworzenie warstwy pomiędzy dwiema kropelkami. W przypadkach, gdy stężenie przekracza CAC, film ten staje się ciągły, utrudniając tym samym udział wody w początkowych etapach koalescencji. Ponadto wielkoskalowe symulacje dynamiki molekularnej są wykorzystywane do badania koalescencji kropelek pokrytych surfaktantem, osadzonych na powierzchniach o różnej zwilżalności. Na uwagę zasługują podobieństwa które obserwuje się pomiędzy koalescencją kropelek osadzonych o równowagowych kątach zwilżania przekraczających $90^\circ$ a swobodnie zawieszonymi kropelkami. Znacząca zmiana dynamiki mostu i mechanizmu transportu masy następuje poniżej kąta zwilżania $90^\circ$, gdy początkowy punkt styku przekształca się w małą, liniową strukturę, wywierającą wyraźny wpływ na różne aspekty procesu koalescencji. Taka konfiguracja pozwala wodzie aktywnie uczestniczyć w koalescencji od samego początku. W końcu zbadano koalescencję osadzonych kropelek polimeru o różnych długościach łańcucha, biorąc pod uwagę wpływ zwilżalności podłoża i lepkości kropel na dynamikę koalescencji i wzrostu mostka. Z przeprowadzonych badań wynika, że obecność podłoża i jego zwilżalność mają istotny wpływ na dynamikę pomostu. Ogólnie rzecz biorąc, zwiększenie długości łańcucha polimeru powoduje zmniejszenie szybkości wzrostu pomostu i szybkości koalescencji.

Podsumowując, niniejsza praca oferuje kompleksowy opis koalescencji kropel, co może odegrać ważną rolę w różnych zastosowaniach, w których szczegółowe zrozumienie zachowania koalescencji kropel, zarówno swobodnie zawieszonych jak i znajdujących się na powierzchniach (siedzących), jest przedmiotem zainteresowania. Ponadto badania te mogą na różny sposób przyczynić się do rozwoju dziedziny. Mogą na przykład zaoferować nowe rozwiązania w przypadkach, gdzie dotychczasowe metody numeryczne lub eksperymentalne nie umożliwiają badania zjawisk na odpowiednio małej skali, czy to na poziomie mikro, nano, czy mniejszym.

# Molecular Dynamics Simulation of the Coalescence of Freely Suspended and Sessile Droplets

by

**Soheil Arbabi**

A Thesis Submitted in Partial Fulfilment
of the Requirements for the Degree of
Doctor of Philosophy

to

Institute of Physics, Polish Academy of Sciences
February, 2024

COPYRIGHT ©2024, BY SOHEIL ARBABI
ALL RIGHTS RESERVED.

# Declaration

I, Soheil ARBABI, declare that this thesis titled, "Molecular Dynamics Simulation of the Coalescence of Freely Suspended and Sessile Droplets", which is submitted in fulfillment of the requirements for the Degree of Doctor of Philosophy, represents my own work except where due acknowledgement have been made. I further declared that it has not been previously included in a thesis, dissertation, or report submitted to this University or to any other institution for a degree, diploma or other qualifications.

Signed: 

Date: February 15, 2024

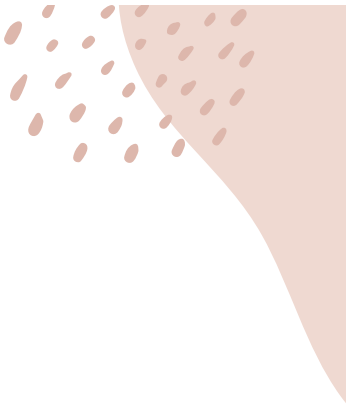

"I'm immensely thankful to my mother, Mersa, and my father, Nasser, for their endless love and support."

# *Acknowledgements*

I would like to express my heartfelt gratitude to Panagiotis Theodorakis and Piotr Deuar for their unwavering support and invaluable guidance throughout my Ph.D. journey. Without their support, it would have been impossible for me to have the opportunity to conduct this research. In fact, their support not only greatly facilitated my academic journey but also enriched my daily life in lovely Poland.

Moreover, I want to express my sincere gratitude to Rachid Bennacer and Zhizhao Che for their guidance and their valuable feedback throughout my PhD journey.

Additionally, I would like to express my gratitude for the support received from the European Union's Horizon 2020 Research and Innovation program, specifically under the Marie Skłodowska-Curie grant agreement number 778104. This support enabled me to collaborate with Elvesys SAS and Professor Rachid Bennacer from ENS Paris-Saclay and afforded me the opportunity to travel to France during my Ph.D. This experience was invaluable, and I gained valuable knowledge and experiences through my collaboration.

Soheil ARBABI
Institute of Physics of the Polish Academy of Sciences
February 15, 2024

# *Acknowledgements*

This thesis was supported by the National Science Centre, Poland, under grant No. 2019/34/E/ST3/00232. I gratefully acknowledge Polish high-performance computing infrastructure PLGrid (HPC Centers: ACK Cyfronet AGH) for providing computer facilities and support within computational grants no. PLG/2020/014344, PLG/2022/015261, PLG/2022/015747, and PLG/2023/016608.

Soheil ARBABI
Institute of Physics of the Polish Academy of Sciences
February 15, 2024

# List of Publications

## JOURNALS:


[1] **Soheil Arbabi**, Piotr Deuar, Mateusz Denys, Rachid Bennacer, Zhizhao Che, Panagiotis E. Theodorakis; Coalescence of surfactant-laden droplets. *Phys. Fluids* **35** 063329 (2023). https://doi.org/10.1063/5.0153676

[2] **Soheil Arbabi**, Piotr Deuar, Mateusz Denys, Rachid Bennacer, Zhizhao Che, and Panagiotis E. Theodorakis. "Molecular dynamics simulation of the coalescence of surfactant-laden droplets." *Soft Matter* **19**, 8070-8080 (2023). https://doi.org/10.1039/D3SM01046E

[3] **Soheil Arbabi**, Piotr Deuar, Rachid Bennacer, Zhizhao Che, and Panagiotis E. Theodorakis, Coalescence of Sessile Aqueous Droplets Laden with Surfactant. *Phys. Fluids* **36**, XXXXX (2024). https://doi.org/10.1063/5.0194816

[4] **Soheil Arbabi**, Panagiotis E. Theodorakis, Coalescence of Sessile Polymer Droplets: A Molecular Dynamics Study. *Macromol. Theory Simul.* **32**, 2300017 (2023). https://doi.org/10.1002/mats.202300017

# Contents

# List of Figures

# List of Tables

# List of Abbreviations

| | |
|---|---|
| **MD** | **M**olecular **D**ynamics |
| **SAFT** | **S**tatistical **A**ssociating **F**luid **T**heory |
| **AA** | **A**ll **A**tom |
| **CG** | **C**oarse **G**rained |
| **TR** | **T**hermal **R**egime |
| **VR** | **V**iscous **R**egime |
| **IR** | **I**nertial **R**egime |
| **DNS** | **D**irect **N**umerical **S**imulation |
| **CAC** | **C**ritical **A**ggregation **C**oncentarion |
| **DFT** | **D**ensity **F**unctional **T**heory |
| **DPD** | **D**issipative **P**article **D**ynamics |
| **EoS** | **E**quation **o**f **S**tate |

# List of Symbols

## Global notations

| | |
|---|---|
| $\sigma_{ij}$ | Effective bead size |
| $\epsilon_{\mathrm{ij}}$ | Interaction strength between any beads of type i and j |
| $r_{ij}$ | Distance between two beads |
| $\tau$ | Time |
| $m$ | Mass |
| $U^{Mie}(r)$ | Mie potential |
| $\lambda_a$ | Mie potential parameter |
| $\lambda_r$ | Mie potential parameter |
| $K_B$ | Boltzmann constant |
| $T$ | Absolute temperature |

## Chapter 2

| | |
|---|---|
| $\gamma$ | Surface tension |
| $\rho$ | Density |
| $t$ | Time |
| $R$ | Droplet radius |
| $R_0$ | Initial droplet radius |
| $b$ | Bridge radius |
| $w$ | Bridge width |
| $Re$ | Reynolds number |
| $\eta$ | Viscosity |
| $V$ | Velocity |

## Chapter 3

| | |
|---|---|
| $A$ | Helmholtz free energy |
| $U(r)$ | Nonbonded potential |
| $\Gamma$ | Surface excess concentration |
| $Z$ | Partition function |

# Chapter 1

# Introduction

## 1.1 Motivation

The coalescence of droplets is a common natural process found throughout nature and it plays a crucial role in processes like understanding how raindrops (Fig. 1.1) come together and their rate of merging [14, 19]. Furthermore, coalescence has numerous practical applications such as inkjet printing, microfluidics, and the purification of water in the separation of crude oil and natural gas [22, 89]. Adding surfactants to droplets can significantly influence coalescence behavior and is essential in various applications. Surfactants can be employed to enhance the stability of droplet boundaries, preventing the merging of tiny droplets and affect the droplet fusion and mixing in microfluidic devices. Furthermore, they can improve the compatibility of the system in biological contexts [12]. Despite considerable research efforts in this area, there are numerous aspects of this process that require further exploration. Until now, investigations involving the coalescence of droplets, whether through experimental, theoretical, or numerical approaches, have predominantly centered on scenarios where pure water or polymer droplets are present [1, 24, 39, 63, 68, 97].

From the perspective of continuum simulations, they have provided primarily explanations and representations of the overall and evolving characteristics of coalescence. However, they often suffer from a lack of adequate resolution at the initial contact point between two droplets, which is also referred to as the 'pinching point' [84]. At the pinching point, the dynamics of bridge and mass transport mechanisms have remained unexplored in numerical methods, primarily due to a singularity that poses challenges for standard numerical approaches. When it comes to experimental methods, high-speed imaging and particle-image velocimetry [21, 40, 61] have been utilized to study the coalescence of surfactant-laden droplets. These techniques have primarily concentrated on portraying the overall characteristics of this phenomenon, similar to numerical simulations. However, due to equipment constraints, capturing the initial stages of coalescence with great precision is a significant obstacle. Both experiments and continuum modeling cannot provide a detailed account of the molecular-level mass transport mechanism and bridge growth dynamics.

Hence, the main goal of this thesis is addressing such issues by using the molecular dynamics method. In particular, we employed a high-fidelity coarse-grained (CG) force-field enabling us to simulate with molecular dynamics the coalescence of surfactant-laden droplets. Coarse-grained molecular dynamics enable us to target larger systems than All-Atom (AA) models, where one attempts to account for every single atom in simulations and which become highly computationally demanding when dealing with droplets and their macroscopic characteristics. Here, the CG methods come into play. In CG methods, each "bead" represents multiple atoms, making simulations computationally efficient compared to those using other MD methods, such as AA models, and allowing the consideration of larger droplets. The use of larger droplets enables the observation of mass transport mechanisms, while minimizing the effects attributable to the finite size of the system. However, the use of CG methods comes with a trade-off, involving the sacrifice of some degrees of freedom and details. For example, in CG models where water molecules ($H_2O$) are considered, a single bead typically represents one or even more water molecules (depending on the CG method). Consequently, studying hydrogen bonds between individual water molecules becomes impossible in such CG models. Therefore, it's essential to exercise caution when selecting a force field that accurately represents important macroscopic properties. When it comes to droplet coalescence, it is crucial for a suitable CG force field to provide precise surface tension values and accurately depict the phase-behaviour of surfactant concentration. In this context, our chosen CG force field (SAFT$\gamma$-Mie CG force field) has undergone rigorous testing and has shown remarkable results [9, 10, 57, 58].

We investigate specific aspects, such as the bridge growth dynamics, mass transport, and water flow, during the coalescence of freely suspended droplets and sessile droplets at each phase of the process. This exploration involves contrasting systems with different types and concentrations of surfactant. Additionally, molecular dynamics methods allow for tracking the movement of each individual particle throughout the coalescence process. This offers exceptional resolution, especially when the bridge formation is observed in the early stages of coalescence, and it provides a comprehensive explanation of the mechanisms involved in mass transport. The investigation of the coalescence of sessile droplets containing surfactants, both below and above the CAC, is another aim of this research. Substrate wettability can have a significant impact on bridge dynamics and mass transport mechanisms. Coalescence on substrates holds substantial industrial applications, and our research aims to provide insights into various aspects of this phenomenon that have remained unclear and unexplored in the existing literature.

In another system, we conducted a study on the coalescence behaviour of polymer droplets with varying chain lengths on substrates that exhibit diverse degrees of wettability. The rationale for exploring different chain lengths is rooted in the fact that an increase in the polymer chain length results in higher viscosity. Therefore, we examined droplets with different chain lengths to investigate the impact of viscosity on the coalescence of sessile droplets.

**Figure 1.1:** Coalescence of raindrops on a glass surface. [1]

## 1.2 Thesis Organization

The content of the subsequent chapters is structured as follows:
**Chapter 2: Background**; In this section, a review of the literature is conducted on the growth dynamics of bridge and the mass transport mechanism during the coalescence of freely suspended and sessile droplets.
**Chapter 3: Methodology**; A summary of the Molecular Dynamics method, with a particular focus on the Coarse-Grained method is provided.
**Chapter 4: Results: Summary of Publications**; In this section the published papers are presented and key findings of each paper are highlighted.
**Chapter 5: Conclusions and Future Work**

[1] Source: Photo by Soheil Arbabi on Unsplash https://unsplash.com/photos/JjIh_9AcVhg and https://unsplash.com/@soheil_rb

# Chapter 2

# Background

## 2.1 Coalescence Mechanisms and Bridge Growth Dynamics

Coalescence of droplets mainly takes place in three different stages:

**1. Droplet Approach** (Figs 2.1a,b): In the initial phase, two distinct droplets approach each other, coming close enough where they start experiencing inter-molecular forces.

**2. Bridge Growth** (Fig. 2.1c): Once the two droplets are positioned close enough, a thin liquid bridge forms between them. Surface tension is responsible for reducing the surface area and thus lowering the overall energy of the system. During the growth phase of the bridge, the liquid bridge passes through various growth regimes. Indeed, the rate of coalescence depends on the dynamics of bridge growth. An explanation of these regimes is one of the main goals of this research. Based on the development of the bridge radius (denoted as $b$), different regimes will be discussed in detail.

**3. Final Reshaping Towards Equilibrium** (Fig. 2.1d): In the final stage, the two droplets merge to form a single, larger droplet. Surface tension forces work to decrease the surface area. Gradually, the system reaches a state of equilibrium, achieving minimization of surface energy.

### 2.1.1 Bridge Growth Dynamics During Coalescence of Freely Suspended Droplets

When two droplets come into close contact without any relative velocity, the primary attractive forces between them are Van der Waals (VDW) forces and electrostatic forces. The VDW forces are the result of fluctuations in electron distributions and tend to bring the droplets closer together, whereas electrostatic forces can also influence their interaction, either attracting or repelling them depending on their charge distribution.

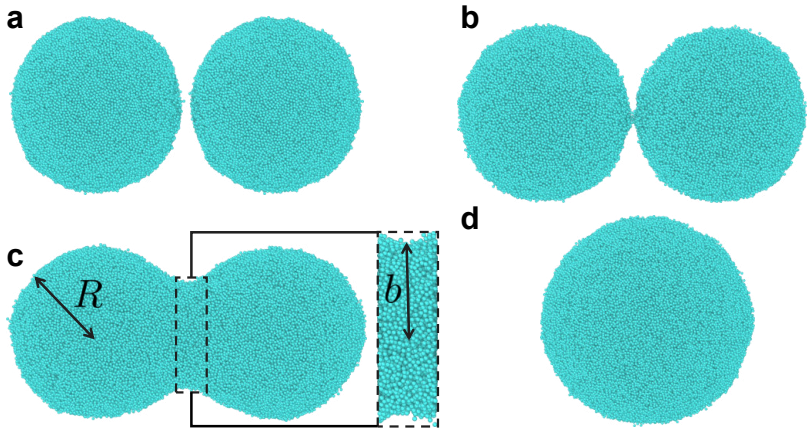


**Figure 2.1:** Stages of coalescence of water droplets with equal size. (a) Initial configuration; (b) Beginning of the bridge formation (Pinching); (c) Bridge growth. The bridge is indicated with a dashed rectangle and a magnified bridge picture with radius $b$ is shown. (d) Final equilibrium configuration after reshaping is completed; The snapshots of the systems were obtained using Ovito software [86].

Viscous forces act as resistance to the coalescence of two liquid droplets at the very beginning of coalescence. Moreover, since the bridge is a highly curved meniscus it creates a capillary pressure gradient where higher pressure in the drop induces a flow towards the bridge. Capillary pressure will be discussed in more detail later in this chapter. Moreover, surface tension effectively maintains the smallest possible liquid-liquid interface between the droplets. The interplay between these attractive and repulsive forces can result in various outcomes, including coalescence, partial coalescence, or even rebounding and separation (in case of droplet collision). The specific behavior observed depends on the unique conditions and parameters of the system. In the context of coalescence, the emergence of a bridge between two droplets occurs within distinct regimes, each under the influence of physical forces and conditions.

The majority of studies on coalescence of droplets have been done on freely suspended droplets in vacuum, air, oil or other liquids [8, 34, 71]. When two droplets are floating inside another fluid in the initial stage of head-on coalescence, a film is created between the two droplets. Once the film thickness decreases to a critical point, VDW forces destabilize the film, leading to film rupture and drainage. The thinning rate depends on the radial pressure gradient within the film, where the Laplace pressure in the film is $\frac{2\gamma}{R}$ , $\gamma$ is surface tension and R is the droplet radius. After the rupture, a bridge connecting two droplets will emerge and grows following a specific power-law scaling, which will be discussed later in this thesis [35]. The dynamic interplay between the various forces involved contributes to the formation of the bridge. Consequently, we will review various studies that have been conducted to explain the dynamics of bridge growth.

**Initial Thermal Regime**: Molecular studies offer high resolution both in time and space, enabling the revelation of an initial regime primarily governed by the thermal fluctuations of molecules. However, this particular regime remains beyond the reach of experimental and continuum studies. Perumanath et al. [68] studied coalescence of two water droplets using an all-atom MD method, and have revealed the emergence of several preliminary bridges due to thermal fluctuations occurring on the droplet's surface. These initial bridges establish connections between the droplets and subsequently expand, thereby highlighting the presence of a thermal phase at the beginning of the coalescence process. In fact, inside the bridge there is a competition between hydrodynamic effects and molecular fluctuation at the pinching stage. Initially, the dominant effect is the thermal motion of molecules. Once a specific point is reached, where the size of the developing bridge exceeds a characteristic thermal length scale, $l_T \approx (k_B T/\gamma)^{1/4} R_0^{/1/2}$, with $R_0$ denoting the initial drop radius, the hydrodynamic regime is recovered. The authors also found that after this initial linear thermal regime, there is a power-law scaling of $b \propto t^{0.5}$ for the entire bridge growth process.

In our studies [4–7], the presence of this initial thermal regime has been identified and characterized not only for pure water droplets, but, also, in the case of surfactant-laden droplets. While Perumanath et al. [68] used an all-atom model to study coalescence of 2D (cylindrical water droplets), we have used a CG model to simulate 3D (spherical-cap droplets) water droplets with and without surfactant, which provides further confidence that this regime is indeed present in the coalescence. However, we were unable to observe linear behavior [68] within this regime, especially in the presence of surfactant [5, 6]. This may be attributed to the complexity introduced by considering 3D droplets, the used CG model, as well as the addition of surfactant molecules.

**The Viscous Regime**: This stage of coalescence corresponds to the Stokes-flow limit, where the dominant forces are macroscopic flows that draw the two droplets together. Gross et al. [28] mentioned that this regime is characterized by the competition between viscous forces and surface tension. To quantify the characteristic velocity in this regime, the parameter $u_c = \gamma/\eta$ is introduced, where $\gamma$ represents surface tension and $\eta$ is the viscosity of the fluid. The dimensionless Reynolds number, $Re$, is defined as $Re = \rho u_c b/\eta = \rho\gamma b/\eta^2$, where $\rho$ is the fluid density, and $b$ is the bridge radius. In the early stages of the process, the radius of the bridge, $b$, is exceedingly small, leading to a very low Reynolds number ($Re \ll 1$). This condition holds regardless of the specific values of $\gamma$ and $\eta$. In summary, since Reynolds number is the ratio of inertial forces to viscous forces, when it is less than one, viscous forces play the main role and that is why this regime is called the viscous regime which can be described by the Stokes equations, in contrast to the inertial regime, $Re \gg 1$, where the Euler equations are valid [28].

However, there is an ongoing debate in the scientific community regarding the validity and significance of viscous regime. Hopper [32] provided an analytical solution for the process of two cylindrical droplets coalescing during viscous sintering. While

sintering may differ from liquid droplets, it can still offer certain understanding. In particular, they revealed that the change in the radius, $b$, of the connecting bridge between the droplets can be approximated by the relation $t \sim -b \ln b^*$, where $b^*$ is defined as $b/R_0$ with $R_0$ being the initial radius of cylindrical droplets. Eggers et al. [24] focused on viscous-dominated coalescence of 3D droplets and obtained $b^* \sim -t^* \ln t^*$ where $b^* < 0.03$ and $t^* = t/\tau_v$ where $\tau_v = \mu R_0/\gamma$ and for larger initial droplet radius ($R_0$) [94].

On the other hand, in experimental studies, a linear scaling is mostly suggested. For example, Thoroddsen et al. [90] found that the viscous behavior in their experiments could be accurately predicted by the linear relationship between the bridge radius ($b$) and time ($t$), expressed as $b \sim t$. Paulsen et al. [64, 65] provided a detailed examination of the coalescence process of droplets containing mixtures of glycerol, water, and NaCl. They employed an ultra-fast electrical method along with a high-speed camera to capture the coalescence events. In their research, they introduced a previously unaccounted-for phase referred to as the inertially limited viscous regime (ILV). They discovered that the initial stages of coalescence cannot be solely described by the traditional Stokes-flow limit. This is because, at the outset of coalescence, the inertia of the droplets plays a significant role and cannot be ignored. This deviation from the traditional Stokes-flow limit[1] occurs when the radius of the bridge is small. However, as the bridge expands, it eventually enters the Stokes regime. The authors highlighted that even when the bridge radius is small and the viscosity is finite (even if it's relatively low), the surface tension force, which is responsible for pulling the two droplets together, is not strong enough to overcome the inertia of the droplets. This observation led them to propose the existence of ILV regime to explain the initial stage of droplet bridging. In the ILV regime, various factors including surface tension, viscous forces, inertia, and the bridge radius was empirically observed to follow a linear scaling with time ($b \sim t$). Burton et al. [16, 94] suggested a crossover length scale from viscous to inertial regime $b_c = \mu(R_0/\rho\gamma)^{0.5}$, which is confirmed by Paulsen and coworkers [63–66, 94], who also found a crossover time-scale as $t_c = \mu^2(R_0/\rho\gamma^3)^{0.5}$.

**The Inertial Regime**: During this phase, the dynamics are characterized by local deformations occurring near the growing bridge. Eggers et al. [24] argued that for $b/R_0 > 0.03$ the bridge flow goes beyond the viscous regime to the inertial and they considered balance between interfacial stress ($\gamma R/b^2$) and dynamic pressure ($\rho v^2$), which leads to a power law of $b \sim (t/\tau_i)^{0.5}$, where $\tau_i = (\rho R_0^3/\gamma)^{0.5}$ [24, 94].

Aarts et al. [1] conducted a study on droplet coalescence within a molecular system characterized by variable viscosity and a colloid-polymer mixture with remarkably low surface tension. Their research challenged the notion that both viscous and inertial regimes are present in all liquids. Specifically, they successfully observed a phenomenon known as purely viscous coalescence, where the radius of the bridge between merging droplets increased linearly with time ($b \sim t$). They also mentioned that,

[1] Stokes flow also referred to as creeping flow, characterizes a fluid flow in which the influence of advective inertial forces are small compared to viscous forces.

in the studied range, no signs of logarithmic correction were observed, as opposed to Hopper et al. [32]. Their findings revealed that the viscous regime characterized by a linear relationship ($b \sim t$) is observable when the Reynolds number is less than one ($Re = \frac{\rho\gamma b}{\eta^2} < 1$). Conversely, when Re exceeds 1, only the inertial regime ($b \sim t^{0.5}$) is detectable. As a result, by defining a crossover at $Re = 1$, they established characteristic length and time scales, experimentally verified as $R_\eta = \frac{\eta^2}{\rho\gamma}$ and $t_\eta = \frac{\eta^3}{\rho\gamma^2}$. Using typical values for pure water, these scales are estimated as $R_\eta = 15nm$ and $t_\eta = 10^{-10}s$. This analysis underscores that, in the case of water, observing the viscous regime is unlikely due to its small characteristic length and time scales. Consequently, the study suggests that witnessing both the viscous and inertial regimes is not a universal phenomenon and may not occur under all conditions in any given liquid.

Nowak et al. [60] studied the coalescence of a surfactant-laden droplet and a water droplet inside silicone oil of various viscosities. In all cases, the bridge growth was characterized by a power law with an exponent of approximately 0.5, and the specific pre-factors varied depending on surfactant concentration and the viscosity of the surrounding liquid. They found that a linear regime (viscous regime) can be observed in experiments only for highly viscous fluids, where the bridge grows linearly with time, represented as $b \sim \gamma/\eta t$. However, in low-viscosity fluids like water, only the inertial regime is observable, and the bridge growth follows a power law given by $b \sim (\frac{R\gamma}{\rho})^{1/4} t^{1/2}$. They also showed that when coalescence happens inside the viscous outer fluid (not in air or vacuum) this equation should be replaced by $b \sim (\frac{R\gamma}{\rho_{out}})^{1/4} t^{1/2}$ where $\rho_{out}$ is the density of the surrounding fluid, while in the case that the inertia of the outer fluid is important, it can be written as $b \sim (\frac{R^3\gamma}{\eta_{out}})^{1/2} t^{1/2}$ where $\eta_{out}$ is viscosity of surrounding fluid.

We were unable to identify any intermediate linear viscous regime in our studies [4–7]. However, adding surfactant leads to more pronounced transition from thermal regime to inertial regime and inertial regime is generally characterized by a power-law behavior with an exponent of 0.5. This transition was observed in all three surfactant types and at various concentrations, which will be presented in more detail in the results section (Chapter 4).

### 2.1.2 Bridge Growth Dynamics of Sessile Droplets

When a liquid droplet is placed on a flat substrate a contact angle, $\theta_s$, is measured, which is the angle between the substrate and the tangent line to the droplet surface. From a macroscopic point of view (Fig. 2.2), force balance at equilibrium is given by the Young–Laplace equation:

$$\gamma_{sg} = \gamma_{lg} \cos\theta_s + \gamma_{sl} \tag{2.1}$$

which means:

$$\cos\theta_s = \frac{\gamma_{sg} - \gamma_{sl}}{\gamma_{lg}} \tag{2.2}$$

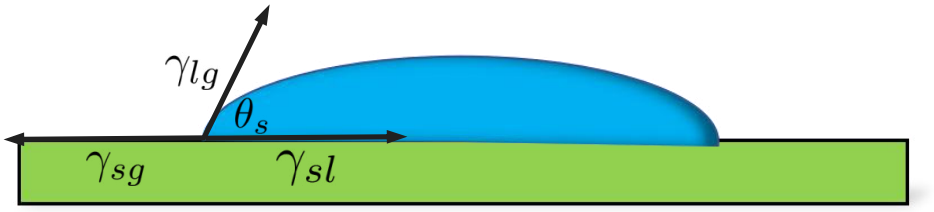


**Figure 2.2:** Schematic of a liquid droplet on a substrate at equilibrium. Contact angle ($\theta_s$) is shown and all three interfacial forces involving the solid ($s$), liquid ($l$) and gas ($g$) are illustrated.

where $\gamma_{lg}$ is surface tension between liquid and gas phases; $\gamma_{sg}$ is the surface tension between substrate and gas, and $\gamma_{sl}$ is the surface tension between substrate and liquid and they are all usually in the unit of mN/m. Measuring contact angles plays a vital role in the examination of wetting phenomena and how surfaces interact with liquids. The nature of the interaction between a liquid and a surface influences the contact angle and it can be categorized based on wettability as follows:

**1. Non-Wettable**: When the equilibrium contact angle exceeds 90° (Fig. 2.3a), in this scenario, the liquid has a tendency to gather into small 'spherical' shapes on the surface, and the substrate is less prone to being wetted by the liquid.

**2. Intermediate Wettability**: In this thesis in the context of the sessile droplets, we define intermediate wettability substrates as those on which the equilibrium contact angle of the droplet is about 90° (Fig. 2.3b).

**3. Wettable**: When the equilibrium contact angle is less than 90° (Fig. 2.3c). In this case, the liquid tends to spread out and wet the surface, forming a liquid film-like structure.

Droplet coalescence on a substrate also follows three main stages, much like what occurs with freely suspended droplets. However, the specific outcomes can vary depending on the substrate's wetting properties. In instances where the substrate is non-wettable by the liquid medium, the formation of a bridge between droplets begins at some distance from the substrate (as illustrated in Fig. 2.3a). In such cases, the dynamics of bridge growth closely resemble the coalescence of suspended droplets. For example, it is shown that the rate of change in the angle of the bridge ($\theta_b$) over time (Fig. 2.3a) in the case of $\theta_s \simeq 140°$ follows the same dynamics as that of the freely suspended droplets [4].

On the contrary, when the substrate is intermediately or highly wettable (as seen in Figs 2.3b and c), the pinching process initiates directly on the substrate. This leads to a distinct coalescence dynamics that is influenced by the presence of the substrate.

It is widely acknowledged that the growth dynamics of bridge width ($w$ in Fig. 2.3c) follows a power-law relationship with an exponent of 0.5, expressed as $w \sim t^{0.5}$ [4, 45, 59, 73]. For instance Ristenpart et al. [73] studied experimentally and theoretically the

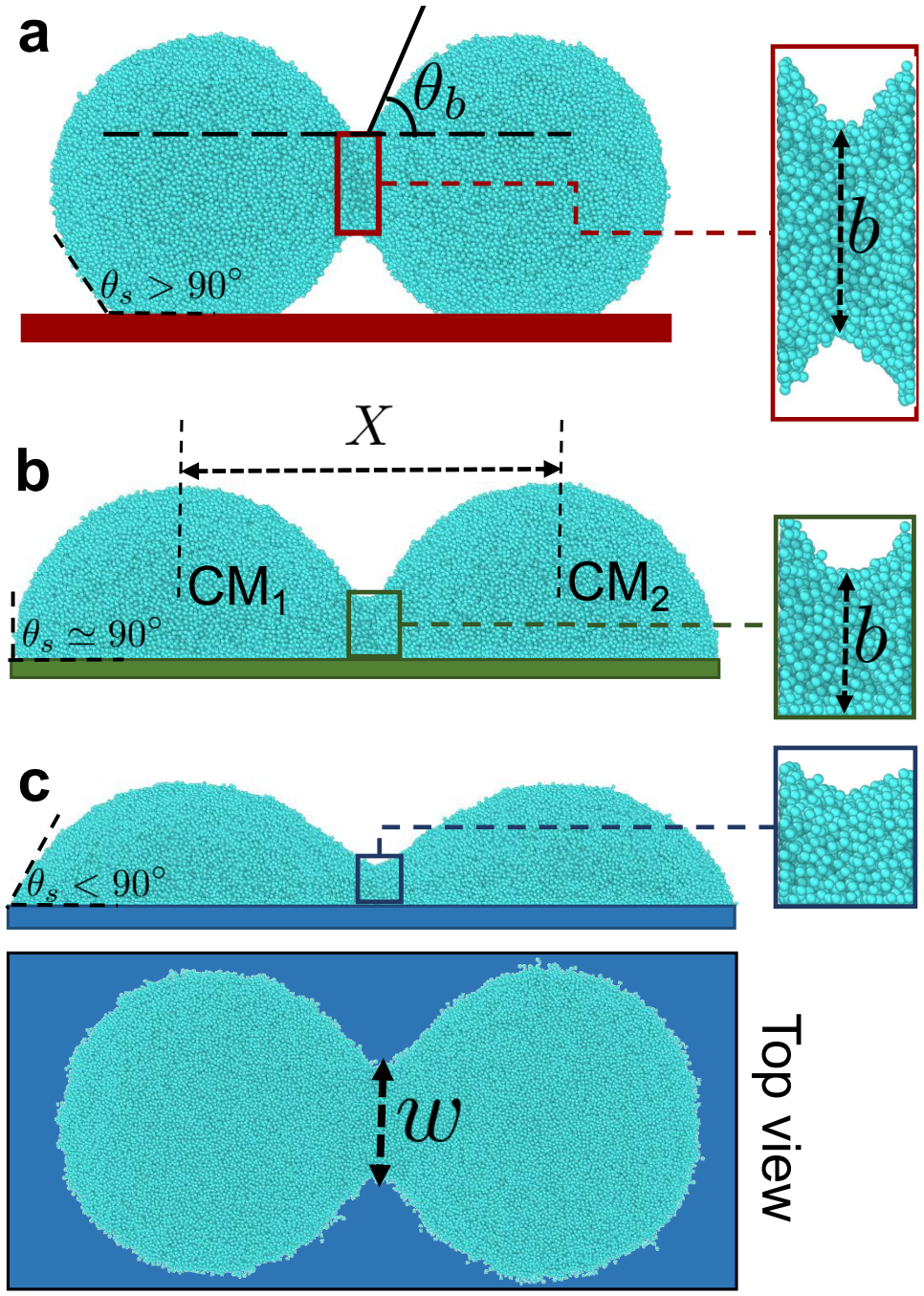


**Figure 2.3:** Bridge formation during coalescence of water droplets on substrates of different wettabilities. (a) Non-wettable substrate ($\theta_s > 90°$); (b) Intermediate substrate ($\theta_s \simeq 90°$); (c) Wettable substrate ($\theta_s < 90°$) and top view of the droplets on wettable substrate. $b$ represents bridge height, $w$ is the bridge width, $\theta_b$ is the angle formed at the bridge and $X$ is the distance between the centers of mass of the two droplets. The snapshot of the systems were obtained using Ovito software [86].

coalescence dynamics of two droplets on a highly wettable substrate. They showed that the width of the bridge scales as $w \sim t^{1/2}$. However, when it comes to bridge height ($b$ in Fig. 2.3), there are varying arguments [26, 73].

When it comes to sessile water droplets, Eddi et al. [23] experimentally studied the coalescence of water drops on substrates with different wettabilities. They demonstrated that on a wettable substrate ($\theta_s < 90^\circ$), the bridge height is characterized by $b \propto t^{2/3}$. However, on intermediate or non-wettable substrates ($\theta_s \geq 90^\circ$), the dynamics shift to $b \propto t^{1/2}$, resembling the behavior of suspended droplets. The bridge dynamics in our MD study [4] on coalescence of sessile water droplets and surfactant-laden droplets is in very good agreement with this experimental study.

The study of coalescence behavior extends beyond water droplets to encompass various other materials, as explored in the literature. For example, Sivasankar et al. [80, 81] conducted a study on the coalescence of microscopic polymeric drops with a density of 1250 kg/m$^3$ on a wettable substrate characterized by $\theta_s = 25^\circ$. They employed a direct numerical simulation (DNS) approach to investigate the collision of droplets and its outcomes under different Weber numbers. The Weber number, denoted as We, serves as a dimensionless parameter for assessing the relative significance of inertial forces compared to surface tension forces in fluid systems. In the context of the collision of two droplets, the Weber number is calculated as $We = \frac{\rho V^2 R}{\gamma}$, where $V$ represents the relative velocity of the droplets during impact. The study examined various Weber numbers, specifically We values of 0, 0.1, and 1, and identified two distinct regimes governing the growth dynamics of the bridge height during coalescence: an early stage and a late stage. In the early stage, the authors reported power-law scaling with exponents of 1/2, 2/3, and 3/1 for We values of 0, 0.1, and 1, respectively. In the late stage of coalescence, a consistent power-law exponent of 1/10 was observed across all cases. Additionally, they observed that the growth of bridge width ($w$) also followed a two-regime power-law pattern.

In another study by Lee et al. [45] , coalescence behavior of macroscopic sessile oil droplets are studied. Authors experimentally studied coalescence of spherical drops (silicone oil) within a diameter range of 100–240 µm. They considered varying contact angles of $10^\circ, 24^\circ, 27^\circ, 56^\circ$ and observed power-law scaling with corresponding exponents of 0.5061, 0.6435, 0.6719, and 0.8612, respectively.

In the scope of coalescence of sessile droplets, we considered the effect of viscosity and substrate on coalescence process. We studied coalescence of sessile polymer droplets [7] and we have found that as the length of the polymer chains increases, which indicates higher viscosity of polymer droplets, the coalescence process becomes significantly slower. We can identify two distinct regimes: an initial thermal regime and an inertial regime. Within the inertial regime, the growth of the bridge follows a power law, but with an exponent that is less than 1/2 for non-wettable surfaces and less than 2/3 for wettable surfaces. These exponents are different from those reported for the coalescence of water or surfactant-laden droplets [4].

Furthermore, in our study of bridge dynamics during the coalescence of sessile surfactant-laden droplets [4], we have confirmed a scaling law with an exponent of approximately 0.5 for bridge width ($w \simeq t^{0.5}$) for both water and surfactant-laden sessile droplets. It is demonstrated that the wettability of the substrate does not affect the growth dynamics of the bridge width. Regarding the bridge height ($b$), the results of our simulations indicate the presence of a power-law scaling relationship, which is influenced by the wettability of the substrate. Specifically, we observe a power-law with an exponent of about 0.5 for non-wettable and intermediate substrates, while for wettable substrates, our results reveal an exponent of $2/3 \simeq 0.7$. In Table. 2.1 our findings [4–7] on bridge dynamics for sessile and suspended droplets are summarized.

**Table 2.1:** Summary of bridge growth dynamics within inertial regime in suspended and sessile droplets in our Studies [4–7].

| **System** | **Bridge width ($w$)** | **Bridge height ($b$)** |
|---|---|---|
| Suspended water and surfactant-laden droplets [5, 6] | $w \sim t^{0.5-0.6}$ | $b \sim t^{0.5-0.6}$ |
| Sessile water and surfactant-laden droplets ($\theta_s \geq 90°$) [4] | $w \sim t^{0.5-0.6}$ | $b \sim t^{0.5-0.6}$ |
| Sessile water and surfactant-laden droplets ($\theta_s < 90°$) [4] | $w \sim t^{0.5-0.6}$ | $b \sim t^{0.6-0.8}$ |
| Sessile polymer droplets ($\theta_s > 90°$) [7] | Not studied | $b \sim t^{0.28-0.38}$ |
| Sessile polymer droplets ($\theta_s < 90°$) [7] | Not studied | $b \sim t^{0.29-0.45}$ |

## 2.2 Mass Transport Mechanism of Surfactant Molecules During Coalescence of Surfactant-Laden Droplets

In this section, we will review some studies on the mass transport mechanism during coalescence, primarily focusing on continuum and experimental methods. Among these studies, Marangoni flow, arising from the gradient of surface tension caused by the presence of surfactants, and capillary flow, predominantly driven by bridge curvature, emerge as the main flows within coalescence. In our studies [4–6], with molecular-level resolution, we track each individual molecule across various regions, including the bulk and surface of each droplet and the bridge between them. By employing this approach, we can elucidate the mass transport mechanism with a very high resolution. Further details on these findings will be discussed in the results section of this thesis.

It is well-established that the addition of surfactants to droplets leads to a reduction in interfacial surface tension and, consequently, delay in the coalescence process [33, 42]. When surfactant is added to a water droplet, the hydrophobic part tends to position toward the droplet's surface. In turn, the surface of the droplet becomes coated with surfactant molecules as depicted in Fig. 2.4b. It is energetically preferable for surfactant to be on the droplet's surface, with some surfactant existing in the form of

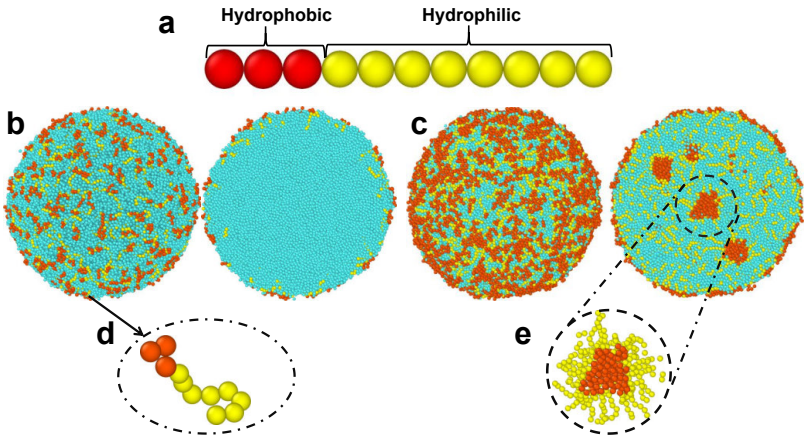


**Figure 2.4:** (a) Schematic of an non-ionic surfactant. Red beads represent the hydrophobic part and yellow beads represent the hydrophilic part; (b) Two surfactant-laden droplets with concentration below CAC; (c) Two surfactant-laden droplets with concentration above CAC; (d) A surfactant monomer on the surface of a droplet; (e) A surfactant aggregate inside the droplet. The snapshot of the systems were obtained using Ovito software [86].

monomers in the bulk of the droplet as well (Fig. 2.4b). Then, when concentration increases and the droplet surface is fully covered, the CAC is reached. At this moment, the surfactant at the surface and the bulk are in a dynamic equilibrium and there is not sufficient space on surface to accommodate a higher amount of surfactant molecules. In such cases, after covering the surface, the remaining surfactant molecules within the bulk of the droplet aggregate together. The aggregation process entails the hydrophobic beads coming together to form a hydrophobic core. In this core, hydrophobic beads try to escape from water, leaving exposed the hydrophilic part of the surfactant (as illustrated in Fig. 2.4e).

While the methodology employed in this study is molecular dynamics, effective forces that are mainly in the scope of continuum methods are summarized below for an overall picture. Nevertheless, even within the continuum framework, accurately quantifying the impact of these effects and characterizing their relative importance alongside surface tension remains a challenge [26], while the mass transport mechanism during coalescence is often influenced by various flows.

Coalescence in this context involves two primary flows: Marangoni and capillary. Both Marangoni flow and capillary flow contribute to the mass transport mechanism during coalescence, influencing the dynamics and behavior of the merging droplets. Below, we will review these main flows and, subsequently, we will examine some experimental studies that visualized and studied the mass transport mechanism during coalescence.

**Capillary Effect:** In the early stages of coalescence, the curvature of the interface undergoes changes as two droplets merge. This alteration in curvature gives rise to capillary

pressure ($\Delta p$). This phenomenon is driven by the Laplace pressure, a pressure jump induced by the curvature of the interface ($R_c$). Consequently, as the droplets approach each other, the radius of bridge curvature decreases, and $\Delta P$ becomes more negative, leading to a capillary attraction force between them. the Laplace pressure is described below as follows:

$$\Delta p = \frac{2\gamma}{R_c} \tag{2.3}$$

or in the case that the curvature radii of the merging droplets (1 and 2) are different:

$$\Delta p = \gamma \left( \frac{1}{R_{c1}} + \frac{1}{R_{c2}} \right) \tag{2.4}$$

**Surfactant-Induced Marangoni Stresses:** Coalescence of surfactant-laden droplets involves a crucial phenomenon known as the Marangoni effect, driven by gradients in surface tension along the interface. When two such droplets come into contact, the presence of surfactants on their surfaces works to reduce the surface tension. However, the non-uniform distribution of surfactants creates a gradient in surface tension. This variation in tension induces tangential stresses on the liquid interfaces called Marangoni stresses.

During the coalescence process, surfactant molecules diffuse in the bulk, and they subsequently adsorb onto the surfaces. Continuum methods are unable to study the molecular-level diffusion of surfactants. However, they can generally explain flow and diffusion using the Advection–Diffusion equation as follows:

$$\rho(\frac{\partial c}{\partial t} + u \cdot \nabla c) = \nabla \cdot (\rho D \nabla c) \tag{2.5}$$

where D is the diffusion coefficient and c the concentration of the solute. This equation considers both convection (transport due to bulk fluid motion) and surfactant diffusion.

In summary, coalescence results in two distinct types of flow: Marangoni flow, which is driven by the gradient of interfacial tension between the droplets at the pinching point and the surface, and bulk flow toward the bridge, which originates from the difference in capillary pressure between the droplet and the curvature of the bridge. The following section will provide a concise summary of key findings from various relevant MD and experimental research papers.

### 2.2.1 MD Study on Mass Transport Mechanisms in the Coalescence of Freely-Suspended and Sessile Surfactant-Laden Droplets

In our studies, using the MD method [4–6], we have investigated the mass transport mechanism of surfactant molecules during the coalescence of surfactant-laden droplets, including both freely suspended droplets and sessile droplets. In the case of freely suspended droplets (Fig. 2.5a, b) [5, 6], pinching starts with surfactant beads, and in concentrations above CAC, a surfactant film between two droplets is created (Fig. 2.5a).

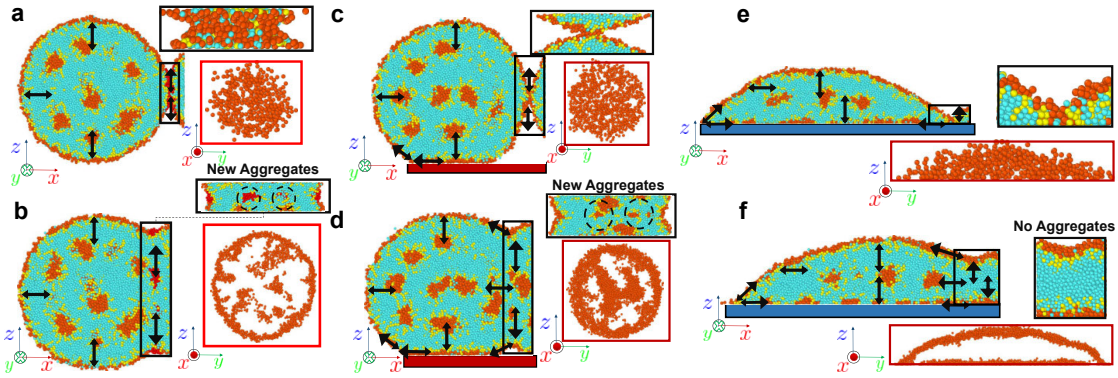


**Figure 2.5:** Mass transport of surfactant molecules of freely suspended droplets (a-b) and sessile droplets (c-f). In all figures a larger arrow-end indicates the dominant direction of surfactant transport and magnified views of the bridge and its cross section on the y–z plane (only hydrophobic beads of surfactant) are shown beside and above each figure (In panels e and f such snapshots are placed beside and below). (a,c,e) Initial stage during coalescence of freely suspended droplets, sessile droplets on a non-wettable, and sessile droplets on a wettable substrate, respectively. (b,d,f) Developed bridge of coalescence of freely suspended droplets, sessile droplets on a non-wettable substrate, and sessile droplets on a wettable substrate, respectively.

The dominant movement of surfactant molecules is from the bulk of the bridge towards the surface of the bridge. However, since there is not enough space on the liquid-gas (LG) surface of the bridge, the bridge surface cannot accommodate all surfactant molecules, resulting in the creation of new aggregates inside the bridge bulk (Fig. 2.5b).

Moreover, our study on sessile droplets [4] reveals that the wettability of the substrate has a significant influence on the mass transport mechanism. When the substrate is non-wettable ($\theta_s > 90°$), pinching starts far from the substrate (Fig. 2.5c), and the coalescence dynamics are very similar to those of suspended droplets. Due to the limited space at the LG interface of the merged droplets (Fig. 2.5d), surfactant from the newly formed aggregates in the bridge bulk cannot be accommodated at the LG interface. Additionally, we observe surfactant transport away from the bridge from the solid-liquid (SL) interface toward the LG surface through the contact line.

The case $\theta_s < 90°$ (Fig. 2.5e) shows a different behavior. The transport toward the LG surface is more pronounced as compared to cases where $\theta_s \geq 90°$. Unlike the preceding instances, the coalescence process does not lead to the formation of new aggregates. This can be ascribed to several factors. Firstly, the smaller amount of surfactant at the bridge in the case of $\theta_s < 90°$ is due to the higher curvature of the droplets. In this scenario, only a small portion of the droplet surfaces come into contact at the contact line. In contrast, for non-wettable substrates, a substantial portion of the surfaces of the two droplets comes into contact, forming a film. Secondly, there is considerably less space in the bridge for aggregates to form from any excess surfactant that does not originate at the bridge's LG surface.

In the results section of this thesis, various features of the coalescence of sessile

droplets will be discussed, including the velocity of approach measured by tracking the distance between the centers of mass of two droplets over time (Fig. 2.3b). Additionally, detailed discussions on bridge dynamics and the mass transport mechanism of surfactants will be presented.

### 2.2.2 Experimental Studies on Mass Transport Mechanism During Coalescence of Droplets

Hack et al. [29] studied coalescence and collision of two droplets with different surface tensions numerically and experimentally. They demonstrated that when the surface tensions of droplets differ, the process of merging droplets exhibits pronounced shape asymmetry in their shape evolution. They propose that capillary waves play a significant role in driving this distinctive shape behavior. Capillary waves are small amplitude, high-frequency oscillations that occur at the interface between two fluids due to surface tension effects. Furthermore, it has been observed that this asymmetry increases as the differences in surface tension between the droplets become more pronounced. In fact, the primary cause of this asymmetry lies in the variations in the amplitudes of the capillary waves on each individual droplet. It is worth noting that they have found that the Marangoni effect can dampen the capillary waves and consequently reduce the overall asymmetry of the merged droplets. This means that when the average surface tension of the droplets is lower, one can expect less asymmetry in the merging process. However, when the surface tension of both droplets are equal (identical droplets), the shape of the merging droplets remains symmetric because the amplitudes and propagation dynamics of the capillary waves on both droplets are identical.

Novak et al. [60, 61] conducted experimental research on the merging of droplets containing both surfactants and water within silicone oils of diverse viscosities. In one study [60], they reported interfacial Marangoni flows and a strong convective flow in case of the coalescence of a surfactant-laden and a surfactant-free water drop. They used dye in water droplet to visualize the bulk motion during the coalescence and the considerable bulk flow is only observed when droplets have different surface tensions. When water droplet is in contact with surfactant-laden droplets due to higher capillary pressure in water droplet the pressure difference drives bulk flow from water droplet to surfactant-laden droplet and at the same time Marangoni flow develops from surfactant-laden droplet to water droplet. The Marangoni flow moves surfactant from surface of surfactant-laden drop to the surface of water drop. Since there is no surfactant in the bulk of the water drop then surfactant will be absorbed from the surface of the water drop to its bulk. Simultaneously, they observed a convection flow that replenishes the surface of a surfactant-covered droplet with surfactant from the bulk of the surfactant-laden droplet. Furthermore, they examined how the viscosity of the surrounding fluid impacts the interfacial flow and confirmed that when a more viscous

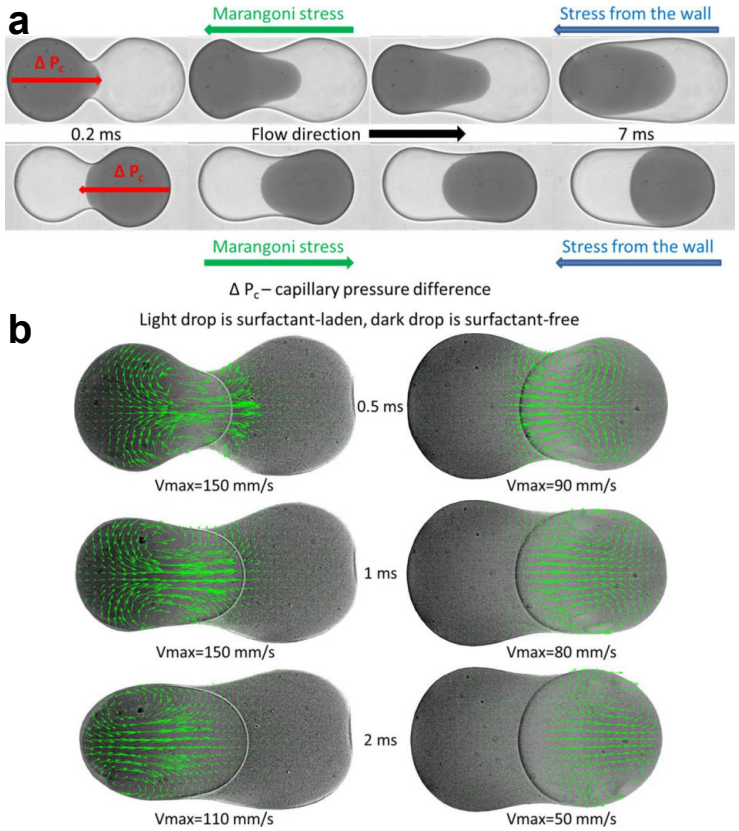


**Figure 2.6:** Coalescence of surfactant-laden droplet and surfactant-free droplet under confinement [40]. (a) Penetration of surfactant-free droplet into surfactant laden droplet due to gradient of capillary pressure which causes asymmetric coalescence. (b) Moreover due to no slip boundary condition on channel walls two vortices are created inside the surfactant-free droplet. The figure is reproduced from Nina M. Kovalchuk and co-workers [40], which investigated the coalescence of surfactant-laden and surfactant-free drops in a microfluidic channel. Reproduced with permission of the publisher, Americal Chemical Society (https://pubs.acs.org/doi/10.1021/acs.langmuir.9b00843#). Further permission related to the material excerpted should be directed to the ACS.

surrounding fluid is present, the interfacial flow proceeds at a slower rate. Moreover, in case of two similar droplets no evidence of Marangoni flow was reported.

In a comparable investigation, Kovalchuk et al. [40] conducted experimental research on the mass transport mechanism during coalescence of a droplet containing surfactant and a pure water droplet within a microfluidic channel (Fig. 2.6). Their findings demonstrate that the surfactant-free droplet penetrates into the surfactant-laden droplet due to capillary pressure-driven flow, which is directed from the water droplet into the surfactant-laden droplet, with a maximum velocity along the axis connecting their centers. In addition, Marangoni flow is generated on the surface. The combination of these flows leads to formation of a film of surfactant-laden liquid spreading over the surfactant-free droplet. It is shown that the rate of penetration depends on various parameters such as drop order penetration inside the tube, where better penetration

is observed when surfactant-laden droplet goes first inside the tube. Moreover, the rate of penetration is enhanced by increasing the interfacial tension difference between the two droplets. They demonstrated that increasing the surfactant concentration from 0.5×CAC to 1×CAC results in an interfacial tension difference ranging from 12 to 22 mN/m, leading to faster and deeper penetration. Due to the no-slip boundary condition on the channel wall, vortices are generated as depicted in Fig. 2.6b. When similar droplets, whether they are both water or both surfactant-laden, coalesce, both droplets equally contribute to the bridge formation. Consequently, four symmetrical convective vortices are generated. This symmetric configuration prevents any exchange of mass between them due to presence of vorticities. In the case of coalescence between droplets with different interfacial tensions, the outcome is influenced by the difference in surface tension and capillary pressure between them. The droplet with the higher capillary pressure or interfacial tension tends to occupy more space within the bridge and can even penetrate into the second droplet (Fig. 2.6). This leads to the formation of only two convective vortices. Notably, these two vortices are consistently located within the water droplet, as observed in the study. However, when the surfactant concentration exceeds the CAC, even transitioning from 1×CAC to 5×CAC does not significantly affect the kinetics of penetration. This is because the saturation of surfactant at the surface with the rest of surfactant remaining in the bulk as monomers and aggregates causes the surface tension to plateau with increasing surfactant concentration.

## 2.3 Summary

In this section, continuum and experimental representative highlights are discussed. Generally, such methods are unable to provide a detailed view of surfactant mass transport and bridge growth dynamics during the coalescence of surfactant-laden droplets. In Chapter 4 of this thesis, we will study the bridge growth dynamics and mass transport of surfactant during the coalescence of suspended and sessile droplets in great detail using the MD method [4–6].

# Chapter 3

# Methodology

## 3.1 Computer Simulation Methods

To describe a fluid system, various approaches are available, covering a range of time and length scales. Table. 3.1 provides an overview of typical length and time scales for these methods at the time of writing. The time and length scales presented in this table are not strict boundaries. They serve as a general outline, typically reflecting common scenarios found in various studies. In practice, the achievable time and length scales can exhibit significant variability. It is important to recognize that as the size of the system under simulation increases, the computational demands also increase significantly. Consequently, researchers should carefully select the appropriate method, level of detail (electronic states, atomic-level detail, molecular interactions, coarse-grained models, mesoscale and macroscale) and length scale based on their scientific objectives and available computational resources. Moreover, there are combined methods, for example, coupling different methodologies offers a means to leverage the strengths of both methods. For example, Smith and Theodorakis [82] provided a perspective on multiscale simulation by combining Molecular Dynamics and Computational Fluid Dynamics (CFD) with a focus on the domain decomposition coupling approach. Each method is applied to a specific segment of the simulation domain in the case of domain decomposition coupling. This approach guarantees the inclusion of molecular detail only where it is essential.

In the case of *ab initio* methods, a complete electronic quantum mechanical description of matter is achieved by solving the wave equations associated with wave mechanics, such as Schrödinger's. However, it is crucial to acknowledge that an essentially exact numerical solution of the Schrödinger equation exists only for systems with a few number of atoms due to the complexity of the many-body wave function. Consequently, this method is impractical for describing the behavior of large droplets. By considering some simplifications, quantum Density Functional Theory (DFT) can provide reasonably accurate simulations for systems containing hundreds of atoms on standard computers or even thousands on large supercomputers. Nevertheless, DFT does have limitations when it comes to accurately describing Van Der Waals (VDW)

forces [18]. This limitation makes it an unsuitable choice even for small droplets, as VDW forces play a pivotal role in coalescence processes. Continuum methods, on the other hand, offer valuable tools for describing the macroscopic behavior of droplets. However, despite numerous fruitful studies, they encounter limitations, particularly in the initial stages of coalescence and the detailed analysis of mass transport mechanisms during coalescence, due to their limited resolution. These limitations which are mentioned in Chapter. 1 encouraged us to consider MD methods, which offer molecular-level resolution of the initial stages of coalescence and can explain the mass transport mechanism of surfactant, which is indispensable in understanding the coalescence of surfactant-laden droplets.

**Table 3.1:** Different computer simulation methods with their typical time and length scales to describe a fluid system.

| **Method** | Time | length |
|---|---|---|
| *Ab initio* | fs - ps | pm-nm |
| DFT | fs-ps | Å-nm |
| AA MD | ps-ns | nm - µm |
| CG MD | ps-s | nm-mm |
| Continuum methods | $\geq$ ms | $\geq$ µm |

In this chapter, we provide a brief review of various molecular dynamics methods, with a specific focus on the chosen CG model, namely, the SAFT$\gamma$-Mie CG force field. Further technical details of the selected force field, such as the parameters, interactions, and bonds, will be provided in the results section (Chapter 4) of this thesis.

## 3.2 Molecular Dynamics Method

By defining the intermolecular interactions, one can calculate the forces acting between every pair of molecules within the system. This force field, in turn, allows for the simulation of the system's dynamic evolution with time. Such simulations provide valuable insights into the structural and thermodynamic characteristics of the system, which enhances our understanding of its behavior. A ubiquitous example of intermolecular interactions is the Lennard-Jones potential Eq. (3.1) [36]

$$U(r_{ij}) = 4\epsilon \left[ \left(\frac{\sigma}{r}\right)^{12} - \left(\frac{\sigma}{r}\right)^{6} \right], \tag{3.1}$$

where r is the distance between the center of mass of each molecule and $\sigma$ and $\epsilon$ are parameters that represent the length scales and energy of the pair interaction, respectively. The force can be obtained through the negative derivative of potential (LJ potential in

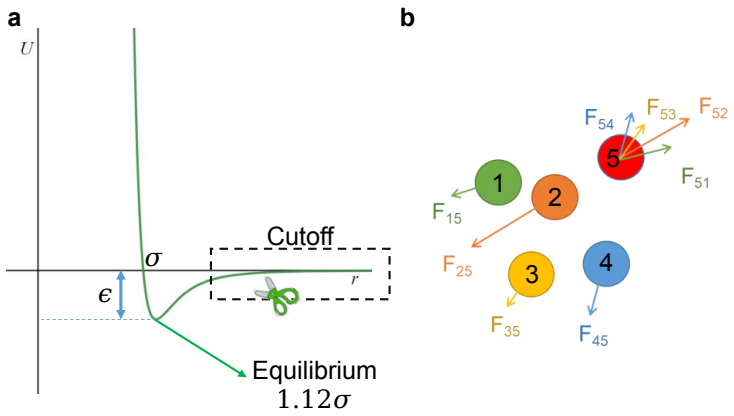


**Figure 3.1:** (a) Lennard-Jones potential. $U(r)$ is the potential energy between two particles at a distance $r$, $\sigma$ is the distance at which the potential energy is zero, $\epsilon$ is the depth of the potential energy well, which characterizes the strength of the attractive interaction between particles. The cutoff determines the distance beyond which pairwise interactions between particles are truncated to reduce computational expense. (b) Schematic of a system of particles and forces acting between every pair of them (forces on particle 5 are shown as well as the counter-force on each of the other particles due to the presence of particle 5).

this case) w.r.t. the distance , which is (Eq. 3.2):

$$F(r) = \frac{24\epsilon}{\sigma}\left[2\left(\frac{\sigma}{r}\right)^{13} - \left(\frac{\sigma}{r}\right)^{7}\right] \tag{3.2}$$

In molecular dynamics simulations, the cutoff serves as a significant parameter in the force-field parametrization. Particularly when dealing with non-bonded interactions like the Lennard-Jones potential. The cutoff for the potential is a parameter that defines the distance beyond which pairwise interactions between particles are truncated to accelerate calculations and reduce computational expense. In general, the choice of the cutoff is made as short as possible to minimize computational costs, as it involves considering a smaller number of nearest neighbor interactions.

### 3.2.1 All-Atom Modeling

In all-atom (AA) or atomistic modeling, each atom is generally considered as a point particle. The parameterization of these force fields based on different particle types involves defining the atom types, their masses, charges, and the potential energy functions that describe their interactions. All of these parameters, including atomic masses, charges, bond parameters, and non-bonded interactions, are collectively referred to as the force field. Several AA force fields exist, such as AMBER [20] which includes various versions such as AMBER94, AMBER96, AMBER99, AMBER14, etc., each with different parameters and refinements for simulating the behavior of amino acids and proteins, as well as CHARMM [15] which includes various versions, such as CHARMM22,

CHARMM27, CHARMM36, and more, each with different parameter sets and improvements to simulate the behavior of biomolecules and other chemical systems. Others include the GROMOS [72] and OPLS [30] family of force fields, which have been developed with their own parameter sets for various types of applications and molecular systems.

Each force field in molecular simulations employs its own unique parameterization method. However, researchers often rely on experimental data to inform the development of force field parameters. These data typically encompass a wide range of information, including structural details, bond lengths, bond angles, and dihedral angles. These experimental findings serve as a foundational basis for calibrating and refining force field parameters to ensure that the simulation accurately represents the behavior of molecules and materials in the real world. Moreover, from finer methods like other AA models, DFT or *ab initio* calculations they obtain accurate energy profiles and electronic properties of molecules and molecular interactions or even for calibrating bonds and angles. This approach provides a rich description of the physics at molecular level. However, several hydrodynamics related topics can hardly be captured by small time and length scales of all-atom models. Furthermore, it introduces numerous intricacies that are likely superfluous when studying the coalescence of droplets. For example, representing each water molecule with three beads (two hydrogen and one oxygen) leads to an abundance of water-water interactions that are not relevant for our research focus. Such unnecessary details can significantly increase computational complexity and impede our ability to simulate large droplets effectively.

### 3.2.2 Coarse Grained Modeling

The complete thermodynamic behavior of a system can be obtained once the Helmholtz free energy, A, of the system is determined. There is a direct relation between Helmholtz free energy and intermolecular interaction as it is shown in Eq. 3.3 [9].

$$\exp(-\beta A) = C \int_V \exp(-\beta U(r)) dr \tag{3.3}$$

$U(r)$ is intermolecular potential and $\beta$ represents $1/k_B T$, $k_B$ is the Boltzmann constant, $T$ is temperature, and C is a constant that incorporates the kinetic contribution. The goal of coarse-graining is to reduce the phase space of $r$ to smaller one ($r_{CG}$) in such a way to be able to find an optimal solution to Eq.3.3 in a reduced phase space as Eq.3.4 [9]:

$$\exp(-\beta A) \simeq C' \int_V \exp[-\beta U_{CG}(r)] dr_{CG} \tag{3.4}$$

By removing certain details in all-atom modeling, we realise a smaller number of calculations, which allows us to access larger time scales and system size. Coarse-grained

modeling can be very helpful in large macromolecules, polymer chains, complex fluids, and surfactants. The choice of the model is also influenced by the length and time scales of the phenomena we aim to study. For instance, in the case of coalescence, one could employ AA models; however, using such models would require waiting much longer than with CG models to observe a complete coalescence. Moreover, when large time scales are required, such as when studying the self-assembly of soft matter, the use of CG methods is crucial [79].

Within CG models, intermolecular potentials and parameterization are established by either adjusting them to data derived from molecular dynamics simulations involving AA, DFT or in general models at a higher level of theory in the case of simulations or from experimental observations. There are several examples of CG models, such as MARTINI [51, 83], which is widely used for the simulation of complex biomolecular systems, SAFT [9, 10, 41, 47, 55–57, 88] which is a CG force-field primarily used for simulating complex fluids, which can contain, for example, polymers and colloids. SPICA [38, 78, 95] which is an empirical CG force-field, was created with the specific aim of accurately replicating thermodynamic properties, including surface tension, density, and distribution functions. SPICA achieves this by drawing insights from all-atom molecular simulations rooted in the CHARMM force-field.

The process of developing a coarse-grained model consists of four key elements [77]: **1.** Selecting the model's level of detail (how coarse it should be); **2.** Determining the arrangement of CG sites based on the geometry/architecture of the molecules; **3.** Specifying the types of interactions to be incorporated; **4.** Fine-tuning these interactions to properly capture selected system properties. Typically, there are two primary approaches to incorporate information into a CG model: Bottom-Up and Top-Down approaches. In the following sections, these approaches will be briefly discussed.

**Bottom-Up Approaches:**

In these approaches, information is passed from any higher resolution model (such as AA, DFT, or *ab initio* methods) to the CG model. In such methods, a standard procedure for coarse-graining involves several key steps. It begins with the collection of data through system sampling; in most cases, coarse-graining requires sampling a reference (high-resolution) system. Subsequently, the collected data is analyzed using a coarse-graining method, resulting in the derivation of coarse-grained potentials. For iterative methods, additional steps may include running coarse-grained simulations and further refining the coarse-grained potentials through successive iterations.

Boltzmann inversion is a commonly applied technique for non-bonded and bonded interactions like bonds, angles, and torsions in molecular simulations. It relies on the structural information of the system and only necessitates the positions of the atoms. The idea in this approach comes from the fact that in canonical ensemble independent degrees of freedom obey the Boltzmann distribution (Eq.3.5) [75].

$$P(q) = Z^{-1} \exp\left[-\beta U(q)\right] \tag{3.5}$$

The symbol Z represents the partition function, which involves a sum or integral over all possible states of the system. Having known $P(q)$, where q is the microscopic state of the system, coarse-grained potential can be defined by inverting the probability distribution of variable q denoted as $P(q)$. The Boltzmann inversion formula is a method used to determine a potential energy function for CG models. It involves relating the potential energy to a desired distribution of a specific structural variable (order parameter, s), such as a bond length, bond angle, or torsion angle. The formula is generally expressed as Eq.3.6.

$$U(s) \approx -k_B T \ln(P(s)) \tag{3.6}$$

where normalization factor, $Z$, would enter the CG potential.

The Iterative Boltzmann Inversion (IBI) method [11, 13] represents a logical progression from the Boltzmann inversion technique. The primary objective of a coarse-grained model is to faithfully replicate distribution functions, such as the spatial distribution of particles, radial distribution functions, or other structural and thermodynamic properties of a reference system. This reference system is often a more detailed or atomistic model, serving as a benchmark for the properties we aim to capture with the coarse-grained model. Through this objective, a systematic enhancement of coarse-grained potentials becomes possible, achieved through an iterative numerical approach [75]. For instance Moore et al. [54] used the standard IBI method to match radial distribution function (RDF of centres of masses of molecules) to derive coarse-grained potentials.

Another approach that can be used in parameterizing a CG model is force matching [75]. In this method the primary goal is not to replicate a variety of distribution functions but rather to achieve a very close match of forces acting on coarse-grained components. This method does not involve iterations, making it computationally less intensive. First, we assume that forces on beads depend on M parameters that can be prefactors of analytical functions, tabulated values of the interaction potentials, or coefficients of splines used to describe these potentials. Then, we assume that the forces acting on the CG beads can be determined by appropriately adjusting the forces acting on individual atoms through a process of reweighting [75].

$$f_i^{ref} = M_i \left[ \sum_a \frac{w_a f_a}{m_a} \right] \tag{3.7}$$

where $M_i$ is the mass of the bead and $a$ denotes number of atoms belonging to that bead and $f_a$ is the force acting on the atom $a$. $w_a$ are mapping coefficients used to obtain the position of the coarse-grained bead ($R_i = \Sigma_a w_a r_a$). By running simulations for a sufficiently extended duration, equations of the form $f_i^{CG}(g_1, g_2, g_3, ..., g_M) = f_i^{ref}$

are obtained for each run and this set of equations can be solved using a least-squares approach. $f_i^{ref}$ represents force on bead $i$ and $g_i$ are parameters of this function that describe the interactions. They can be pre-factors of analytical functions or tabulated values of the interaction potentials. $f_i^{CG}$ is CG representation of this force. Through validation and comparison, a set of forces acting on beads are obtained, which constitute the CG force-field.

**Top-Down Approaches:**

In these approaches, we consider macroscopic properties and we try to figure out what is the intermolocular potential that can produce these properties. While top-down approaches can be used for the intermolecular interactions, these can be combined with bottom-up approaches to determine intramolecular potentials for bonds and angles, as for example in the case of the MARTINI force-field [51, 83].

**MARTINI Force-Field**

MARTINI [51, 83] employs a top-down method involving thorough adjustment of the non-bonded interactions among chemical components based on experimental information, especially thermodynamic data like oil-to-water partitioning coefficients [52]. The mapping in MARTINI model in general is based on four-to-one approach where on average four heavy atoms and associated hydrogen atoms are represented as a unit interaction center (bead). Non-bonded interactions between beads in MARTINI are described by the Lennard-Jones (LJ) 12-6 potential (Eq.3.1).

This involves calculating the free energy of hydration, the free energy of vaporization, and the partitioning free energies between water and various organic phases for all 18 distinct coarse-grained particle types in MARTINI2 and 29 distinct coarse-grained particle types in MARTINI3 [83]. The MARTINI model for specific systems accurately replicates the expected patterns in free energies of hydration and vaporization [52]. Moreover, the MARTINI model particularly has been validated for several different lipids [50], peptides and proteins [27, 37, 53, 67], polymers [44, 74], sugars [93], DNA [91], RNA [96], various solvent [92] , carbohydrates [49] and a wide range of other types of materials (mostly bio-materials).

In coalescence of droplets, surface tension plays a significant role that is why we compared the surface tension of pure water in MARTINI versions 2 and 3, and, also, explored the effect of the potential cutoff on the surface tension (Table. 3.2). In general, CG models tend to underestimate surface tension compared to all-atom and experimental measurements, primarily due to a smaller number of interactions. As a result, increasing the cutoff leads to larger surface tension. Our results (Table. 3.2) indicate that MARTINI version 2, using a cut-off of 35Å, closely approximates the experimental surface tension of water ($71.99 \pm 0.05$) at room temperature ($25^{\circ}C$) [62]. However, the MARTINI force-field could not provide a satisfactory agreement with the experimental phase behavior of our selected surfactants. That is why we have opted to consider the

SAFT $\gamma$-Mie force-field, which has undergone evaluation for various properties, such as surface tension and phase behavior of our selected surfactants.

**Table 3.2:** Comparison of MARTINI versions 2.2 and 3.0, examining their surface tension on pure water under various cut-offs. The surface tension of water–air at 25° is 71.99±0.05 [62].

| **MARTINI version** | Cut-off (Å) | Surface Tension (mN/m) |
|---|---|---|
| 3.0 | 11 | $27.11 \pm 0.81$ |
| 3.0 | 25 | $50.20 \pm 0.80$ |
| 3.0 | 35 | $50.49 \pm 0.78$ |
| 2.2 | 11 | $31.02 \pm 0.79$ |
| 2.2 | 25 | $56.04 \pm 0.84$ |
| 2.2 | 35 | $85.80 \pm 0.84$ |

### SAFT $\gamma$-Mie Force-Field

SAFT is a CG force field that maps the size, energy, and range of beads to expected macroscopic properties (it matches to macroscopic properties, first and also second derivatives of the free energy). It is a top-down approach where a molecular-based equation of state is employed to get an effective coarse-grained intermolecular potential that reproduces macroscopic thermodynamical properties [9, 10]. SAFT deals with the classical idea how to build an equation of state. The SAFT equation of state [17] is employed in the field of thermodynamics and the modeling of fluid phases to anticipate the actions of fluids, including polymers, colloids, and molecules that associate with one another. Moreover, SAFT also employs a more general LJ potential form, known as the Mie potential (Eq. 3.8), as it provides a greater number of parameters. This allows for a more effective fitting of the equation of state (EoS) to experimental data. In this approach, essentially, there is a cyclic process involving theory (Equation of State), experimental data, and simulations (MD or Monte Carlo), which is used to parameterize the Mie potential and refine the SAFT coarse-grained force field.

In the SAFT-$\gamma$ Mie approach [9, 10, 56–58] interactions between two spherical segments can be represented with the Mie potential (Eq.3.8) [46].

$$u^{Mie} = C\epsilon \left[ \left(\frac{\sigma}{r}\right)^{\lambda_r} - \left(\frac{\sigma}{r}\right)^{\lambda_a} \right] \tag{3.8}$$

where $\lambda_r$ and $\lambda_a$ are the exponents of the potential. $\lambda_a$ is constant but $\lambda_r$ is used as a fitting parameter and C is defined as follows:

$$C(\lambda) = \frac{\lambda_r}{\lambda_r - \lambda_a} \left(\frac{\lambda_r}{\lambda_a}\right)^{\frac{\lambda_a}{\lambda_r - \lambda_a}} \tag{3.9}$$

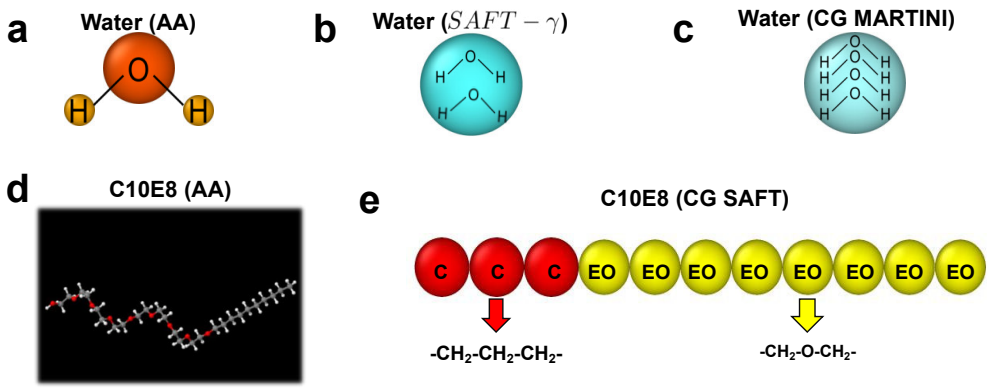


**Figure 3.2:** (a) All-atom representation of a water molecule; (b) Coarse-grained representation of two water molecules by one SAFT bead; (c) Coarse-grained representation of four (MARTINI) water molecules; (d) All-atom representation of a C10E8 molecule [Source: Chemical Compounds Deep Data Source (CCDDS; https://www.molinstincts.com) based on 41 patented SQN and QN technology commercialized into Mol-Instincts database and ChemRTP, ChemEssen, Inc (2022)]; (e) Coarse-grained representation of a C10E8 molecule in SAFT force-field. A hydrophobic alkane CG 'C' bead represents a $-CH_2-CH_2-CH_2-$ group of atoms while a hydrophilic CG 'EO' bead represents $-CH_2-O-CH_2$ group.

To parameterize the SAFT-$\gamma$ force field, there are different parameters that are adjustable including the level of coarse-graining (how many atoms should represent each bead), $\epsilon$, $\sigma$, $\lambda_r$ and $\lambda_a$ set to 6 (which is because this is a physical exponent that describes the dispersion interactions between particles). For this parameterization process, macroscopic data such as vapor-liquid densities and vapor pressures are commonly utilized, although other macroscopic properties can also be considered. By utilizing this macroscopic data, one can determine the parameters necessary for the EoS and the force field. Moreover, the validity of the force-field is checked in practice in the simulations and when the simulations are able to reproduce the target properties, then, the theory is in practice validated.

As mentioned, increasing the number of parameters in the Mie potential enhances its versatility compared to the Lennard-Jones 12-6 potential, which is employed in the MARTINI force field. The 12-6 LJ potential has demonstrated remarkable success in various applications, showcasing its outstanding versatility. In this thesis, for instance, when examining sessile polymer droplets [7], we employed a 12-6 LJ potential. We utilized a physics-based CG force field for polymer chains, implementing a standard bead–spring model. However, it is essential to acknowledge that, like any model, it may encounter challenges. For instance, it is reported that it cannot simultaneously reproduce saturated liquid densities and vapor pressure of n-alkanes [9, 69]. Moreover, it is mentioned that the Lennard-Jones 12-6 potential often struggles to accurately represent fluid-phase equilibria and is known to provide poor representations of vapor-pressure curves [85].

The force field selected for the study of surfactant-laden droplets in this thesis is based on the SAFT-$\gamma$ Mie EoS, which has been demonstrated to provide convincing

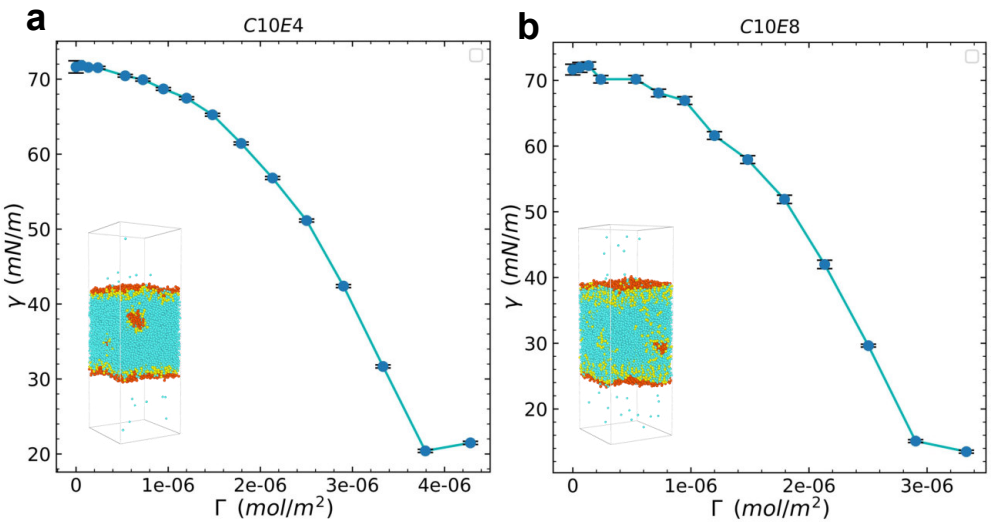


**Figure 3.3:** Surface tension isotherms as obtained by the simulations in the planar limit for the (a) C10E4 and (b) C10E8 surfactants, using SAFT force field. The insets show slab of water laden with surfactant (above CAC).

agreement with experimental results, including phase diagrams, surface tension of the chosen surfactants, and other properties such as contact angles [87, 88]. In Figs 3.2 a-c, we present a comparison between the water models in atomistic and CG systems of MARTINI and SAFT. Additionally, we provide a comparison between the C10E8 surfactant in all-atom and SAFT models (Figs 3.2 d-e). C10E8 is a large molecule, and considering an atomistic model for it, would be computationally extremely expensive computationally. However, the SAFT CG model allows us to handle large systems with good accuracy and lower computational costs. In Fig. 3.3, we present examples of surface tension isotherms versus surface excess concentration ($\Gamma$ [mol/m$^2$]), with the latter being the area-related concentration of a surfactant at the surface or interface for a liquid-vapor (LV) interface. These data demonstrate a close agreement with experimental data [3, 43] and previously obtained simulation results [47, 48, 87, 88]. In addition, it has been demonstrated that the SAFT coarse-grained model is capable of accurately replicating the complex phase behavior of several different surfactants including C10E4, C10E8, Silwet-L77, spanning from extremely low concentrations to the formation of aggregates, and even extending to the presence of lamellar phases at higher concentrations.

## 3.3 Summary

In this section, we briefly reviewed CG MD methods and discussed different CG models. Using CG models make it possible to target large droplets to observe changes in

shape of the droplet, avoiding effects that would be attributed to the small size of the droplets, and, also, be able to track the motion of surfactants at adequately large concentrations. Moreover among several existing successful CG methods checking surface tension and phase diagram of surfactant molecules convinced us that SAFT is the best possible choice to study coalescence of surfactant-laden droplets. The SAFT force-field has demonstrated successful testing not only in surface tension and surfactant phase diagrams of non-ionic surfactants but also in various studies involving different liquid and surface phenomena, as well as long-chain molecules and biomolecules. Examples of its application include liquid crystals [70], polymers [25], cryogenic fluids [2], water-oil interfacial tensions [31], super spreading surfactants [88]. Furthermore, it has been shown that this force field reproduces well the contact angles of water [76, 88].

# Chapter 4

# Results: Summary of Publications

## 4.1 Coalescence of Surfactant-laden Droplets

### 4.1.1 Summary of Key Findings of This Publication:

In this work, we studied coalescence of freely suspended surfactant-laden droplets. We considered a non-ionic surfactant (C10E4) with various concentrations below and above CAC. We presented the mass transport mechanism, bridge growth dynamics, and water flow during coalescence using molecular dynamics. The key findings of this work are summarized as follows:

- Demonstrating the initiation of pinching involves hydrophobic beads within surfactant molecules. After pinching, a hydrophobic film will be created between two droplets, which delays the participation of water molecules in the process.
- The dominant movement inside the bridge is the transport of surfactants from the bridge bulk to the bridge surface. However, since coalescence is a dynamic process there is not enough time and there is lack of enough space on bridge surfaces for all surfactants, which mainly come from the droplets' surfaces. Hence, some surfactant, previously part of the surfaces of the droplets, creates new aggregates inside the bridge bulk.
- The bridge initially undergoes growth within a Thermal Regime (TR), followed by a subsequent inertial regime characterized by a power law with an exponent of approximately 0.5. We have shown that higher concentration of surfactant leads to larger TR and the transition between TR and intertial regime (IR) is more pronounced in the presence of surfactant.
- Strong water flow towards the bridge is found in the case of coalescence of water droplets, which is hindered by adding more surfactant.

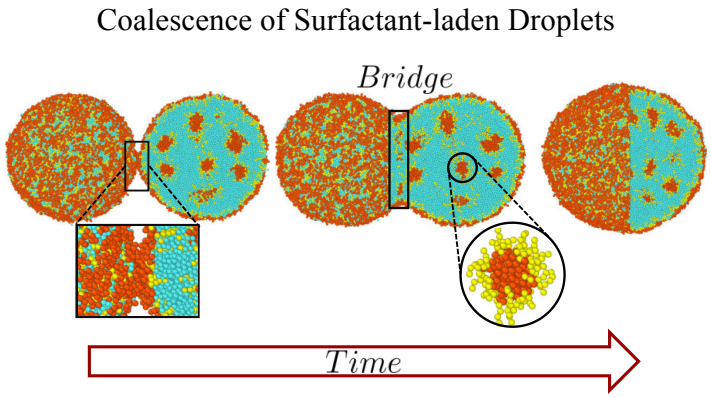


**Figure 4.1:** Stages of Coalescence of surfactant-laden droplets, Reproduced from [Soheil Arbabi, Piotr Deuar, Mateusz Denys, Rachid Bennacer, Zhizhao Che, Panagiotis E. Theodorakis, *Coalescence of surfactant-laden droplets*, Phys. Fluids., **35** 063329 (2023) https://doi.org/10.1063/5.0153676], with the permission of AIP Publishing.

### 4.1.2 Details of Publication

**Coalescence of Surfactant-laden Droplets**

PDF version of this publication is reproduced from [Soheil Arbabi, Piotr Deuar, Mateusz Denys, Rachid Bennacer, Zhizhao Che, Panagiotis E. Theodorakis, Coalescence of surfactant-laden droplets, Phys. Fluids **35,** 063329 (2023). https://doi.org/10.1063/5.0153676], with the permission of AIP Publishing.

Soheil Arbabi

Institute of Physics, Polish Academy of Sciences (PAN)

Theoretical Physics Division (ON5),

Al. Lotników 32/46 02-668 Warsaw, Poland

arbabi@ifpan.edu.pl

# STATEMENT

I declare that I am the co-author of the publication:

Coalescence of surfactant-laden droplets, Phys. Fluids., **35**, 063329 (2023),

https://doi.org/10.1063/5.0153676

I contributed equally to the conceptualization. I took the lead role in data curation, analysis, investigation, methodology, simulations, validation, visualization and writing the draft. In addition, I played an equal part in review, and editing tasks.

signature:

INSTYTUT FIZYKI
POLSKIEJ AKADEMII NAUK

dr hab. Piotr Deuar
Head of the Quantum Noise group
Institute of Physics, Polish Academy of Sciences (PAN)
Theoretical Physics Division (ON5),
Al. Lotników 32/46 02-668 Warszawa, Poland
deuar@ifpan.edu.pl

# STATEMENT

I declare that I am the co-author of the publication:

*Coalescence of surfactant-laden droplets*
Phys. Fluids., **35**, 063329 (2023), https://doi.org/10.1063/5.0153676

My contributions included supporting mr Arbabi in analysis, conceptualization, as well as participation in discussions, reviewing and editing the draft, and co-supervision.

signature:

INSTYTUT FIZYKI
POLSKIEJ AKADEMII NAUK

Dr.Mateusz Denys

Institute of Physics, Polish Academy of Sciences (PAN)

Theoretical Physics Division (ON5),

Al. Lotników 32/46 02-668, Warsaw, Poland

# STATEMENT

I declare that I am the co-author of the publication:

Coalescence of surfactant-laden droplets, Phys. Fluids **35**, 063329 (2023),

https://doi.org/10.1063/5.0153676

My contribution was supporting in Conceptualization and participation in discussions and reviewing the draft.

Signature:

Département Génie Civil et environnement
e-mail : rachid.bennacer@ens-Paris-Saclay.fr
www.dgc.ens-paris-saclay.fr

# STATEMENT

I declare that I am the co-author of the publication:

Coalescence of surfactant-laden droplets, Phys. Fluids., 35, 063329 (2023),

https://doi.org/10.1063/5.0153676

My contributions included supporting conceptualization, participating in discussions, and reviewing/editing the draft.

Paris-Saclay le 07/12/2023

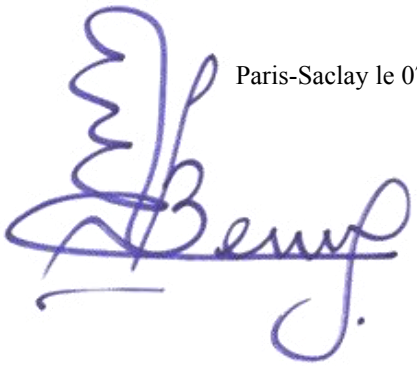

**Tianjin University**

Zhizhao Che, PhD, Professor

State Key Laboratory of Engines, Tianjin University

135 Yaguan Road, Haihe Education Park,

Tianjin, 300350, China

Email: chezhizhao@tju.edu.cn

# STATEMENT

I declare that I am the co-author of the publication:

Coalescence of surfactant-laden droplets, Phys. Fluids., **35**, 063329 (2023),

https://doi.org/10.1063/5.0153676

My contribution involved supporting conceptualization, participating in discussions, and reviewing/editing the draft.

signature: 

Dr hab. Panagiotis Theodorakis
Division of Theoretical Physics (ON5)
Al. Lotników 32/46
02-668 Warsaw, Poland

# STATEMENT

I declare that I am the co-author of the publication:

- **Coalescence of surfactant-laden droplets**
  S. Arbabi, P. Deuar, M. Denys, R. Bennacer, Z. Che, P. E. Theodorakis
  *Phys. Fluids* **35,** 063329 (2023), doi:10.1063/5.0153676

My contribution was supervising the project, helping in the interpretation of the results, and in manuscript writing.

Warsaw, 09.12.2023
Panagiotis Theodorakis

Soheil Arbabi

Institute of Physics, Polish Academy of Sciences (PAN)

Theoretical Physics Division (ON5),

Al. Lotników 32/46 02-668 Warsaw, Poland

arbabi@ifpan.edu.pl

# STATEMENT

I declare that I am the co-author of the publication:

Molecular dynamics simulation of the coalescence of surfactant-laden droplets, Soft Matter, **19**, 8070-8080 (2023), https://doi.org/10.1039/D3SM01046E

I contributed equally to the conceptualization. I took the lead role in data curation, analysis, investigation, methodology, simulations, validation, visualization and writing the draft. In addition, I played an equal part in review, and editing tasks.

signature:

INSTYTUT FIZYKI
POLSKIEJ AKADEMII NAUK

dr hab. Piotr Deuar
Head of the Quantum Noise group
Institute of Physics, Polish Academy of Sciences (PAN)
Theoretical Physics Division (ON5),
Al. Lotników 32/46 02-668 Warszawa, Poland
deuar@ifpan.edu.pl

# STATEMENT

I declare that I am the co-author of the publication:

*Molecular dynamics simulation of the coalescence of surfactant-laden droplets*,
Soft Matter, **19**, 8070-8080 (2023), https://doi.org/10.1039/d3sm01046e

My contributions included supporting mr Arbabi in analysis, conceptualization, as well as participation in discussions, reviewing and editing the draft, and co-supervision.

signature:

INSTYTUT FIZYKI
POLSKIEJ AKADEMII NAUK

Dr.Mateusz Denys

Institute of Physics, Polish Academy of Sciences (PAN)

Theoretical Physics Division (ON5),

Al. Lotników 32/46 02-668, Warsaw, Poland

# STATEMENT

I declare that I am the co-author of the publication:

Molecular dynamics simulation of the coalescence of surfactant-laden droplets, Soft Matter, **19**, 8070-8080 (2023), https://doi.org/10.1039/D3SM01046E

My contribution was supporting in Conceptualization and participation in discussions and reviewing the draft.

signature:

Département Génie Civil et environnement
e-mail : rachid.bennacer@ens-Paris-Saclay.fr
www.dgc.ens-paris-saclay.fr

# STATEMENT

I declare that I am the co-author of the publication:

Molecular dynamics simulation of the coalescence of surfactant-laden droplets, Soft Matter, **19**, 8070-8080 (2023), https://doi.org/10.1039/D3SM01046E

My contributions included supporting conceptualization, participating in discussions, and reviewing/editing the draft.

Paris-Saclay le 07/12/2023

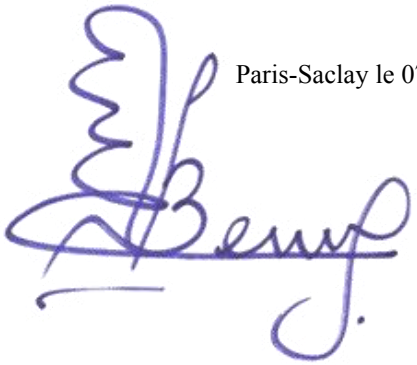

Tianjin University

Zhizhao Che, PhD, Professor

State Key Laboratory of Engines, Tianjin University

135 Yaguan Road, Haihe Education Park,

Tianjin, 300350, China

Email: chezhizhao@tju.edu.cn

# STATEMENT

I declare that I am the co-author of the publication:

Molecular dynamics simulation of the coalescence of surfactant-laden droplets, Soft Matter, **19**, 8070-8080 (2023), https://doi.org/10.1039/D3SM01046E

My contribution involved supporting conceptualization, participating in discussions, and reviewing/editing the draft.

signature: 

Dr hab. Panagiotis Theodorakis
Division of Theoretical Physics (ON5)
Al. Lotników 32/46
02-668 Warsaw, Poland

# STATEMENT

I declare that I am the co-author of the publication:

- **Molecular dynamics simulation of the coalescence of surfactant-laden droplets**
  S. Arbabi, P. Deuar, M. Denys, R. Bennacer, Z. Che, P. E. Theodorakis
  *Soft Matter* **19,** 8070 (2023), doi: 10.1039/d3sm01046e

My contribution was supervising the project, helping in the interpretation of the results, and in manuscript writing.

Warsaw, 09.12.2023
Panagiotis Theodorakis

## 4.3 Coalescence of Sessile Aqueous Droplets Laden with Surfactant

### 4.3.1 Summary of Key Findings of this Publication:

In this paper, we explored the coalescence of sessile surfactant-laden droplets on various substrates, including wettable ($\theta_s < 90^\circ$), intermediate ($\theta_s \simeq 90^\circ$), and non-wettable ($\theta_s > 90^\circ$) substrates. We employed the SAFT CG force field to study sessile water droplets and surfactant-laden droplets both below and above the CAC. We compared the mass transport mechanism of surfactant molecules and bridge dynamics on three different substrates during the coalescence. Additionally, we studied the dynamics of the contact angle on the bridge ($\theta_b$), density profile, and velocity of approach between the coalescing droplets. The key findings of this work are summarized as follows:

- Sessile droplets with $\theta_s \geq 90^\circ$ share similarities with freely suspended droplets. For contact angle of $\theta_s \simeq 140^\circ$ our results show that coalescence behaves practically as if they were freely suspended. The pinching region and bridge formation begin at a distance from the substrate, and only later does the bridge region come into contact with the substrate. For instance, a comparison of the bridge angle ($\theta_b$) with freely suspended droplets reveals very similar behavior. Moreover, mass transport mechanisms in this case exhibit similarities with freely suspended droplets, with the predominant movement of surfactant molecules from the bulk of the bridge to the surface of the bridge. The creation of a surfactant film in the pinching process (in the case of concentrations above the CAC) and the formation of new aggregates within the bridge bulk have been reported in this scenario. Regarding the bridge dynamics, the exponents for the power law (in the inertial regime) are approximately 0.5, consistent with observations in freely suspended droplets.
- In the case of an intermediate scenario ($\theta_s \simeq 90^\circ$), the bridge dynamics closely resemble those of non-wettable substrates; however, it grows slightly slower due to pinching initiating on the substrate. Concerning the mass transport mechanisms, the involvement of water in the pinching process is marginally higher, but overall, the mass transport mechanism of surfactant molecules within the bridge is akin to that of non-wettable substrates.
- Sessile droplets with $\theta_s < 90^\circ$, on the other hand, exhibit markedly different behavior in terms of mass transport mechanisms and bridge dynamics. We have investigated contact angles of approximately $50^\circ$ and $70^\circ$ for both water droplets and surfactant-laden droplets, both below and above CAC. Overall, it is demonstrated that when the contact angle is above $90^\circ$, the bridge height ($b$) grows with an exponent of 0.5 within the inertial regime. However, in the case of wettable

substrates ($\theta_s < 90^\circ$), an exponent of $2/3$ is observed. Regarding the mass transport mechanism, wettable substrates exhibit increased water participation in the pinching process compared to non-wettable substrates. A notable result is the absence of newly formed aggregates as the bridge grows during coalescence in the case of wettable substrates.

- We calculated the velocity of approach between two droplets, and it was observed that the velocity is smaller when wettable substrates are used, irrespective of surfactant concentration.

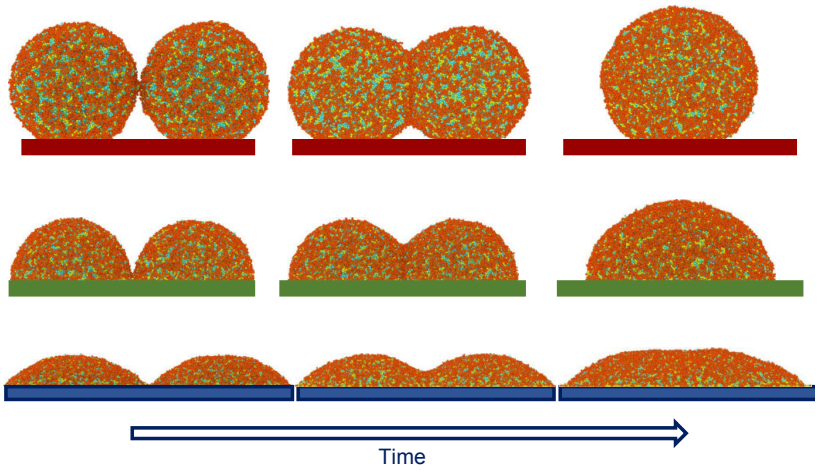


**Figure 4.3:** Coalescence of Sessile Aqueous Droplets Laden with Surfactant. Reprinted from [ Soheil Arbabi, Piotr Deuar, Rachid Bennacer, Zhizhao Che, and Panagiotis E. Theodorakis, Coalescence of Sessile Aqueous Droplets Laden with Surfactant. Phys. Fluids **36**,(2024), https://doi.org/10.1063/5.0194816].

### 4.3.2 Details of Publication

**Coalescence of Sessile Aqueous Droplets Laden with Surfactant**

PDF of accepted version of this publication is reproduced from [Soheil Arbabi, Piotr Deuar, Rachid Bennacer, Zhizhao Che, and Panagiotis E. Theodorakis, Coalescence of Sessile Aqueous Droplets Laden with Surfactant. Phys. Fluids **36**,(2024), https://doi.org/10.1063/5.0194816].

Soheil Arbabi

Institute of Physics, Polish Academy of Sciences (PAN)

Theoretical Physics Division (ON5),

Al. Lotników 32/46 02-668 Warsaw, Poland

arbabi@ifpan.edu.pl

# STATEMENT

I declare that I am the co-author of the publication:

*Coalescence of sessile aqueous droplets laden with surfactant, S. Arbabi, P. Deuar, R. Bennacer, Z. Che, P. E. Theodorakis Fluid Phys. 36,(2024), doi : 10.1063/5.0194816*

I contributed equally to the conceptualization. I took the lead role in data curation, analysis, investigation, methodology, simulations, validation, visualization and writing the draft. In addition, I played an equal part in review, and editing tasks.

signature:

INSTYTUT FIZYKI
POLSKIEJ AKADEMII NAUK

dr hab. Piotr Deuar, prof. IF PAN
Head of the Quantum Noise group
Institute of Physics, Polish Academy of Sciences (PAN)
Theoretical Physics Division,
Al. Lotników 32/46 02-668 Warszawa, Poland
deuar@ifpan.edu.pl

# STATEMENT

I declare that I am a co-author of the publication:

*Coalescence of Sessile Aqueous Droplets Laden with Surfactant*, Phys. Fluids, **36,** (2024)
S. Arbabi, P. Deuar, R. Bennacer, Zhizhao Che, P. E. Theodorakis
https://doi.org/10.1063/5.0194816

My contributions included support of Mr Soheil Arbabi in analysis, conceptualization participation in discussions, as well as reviewing and editing the draft.

signature:

Prof. Rachid BENNACER
Univ. Paris-Saclay
4 Avenue des Sciences,
91190 Gif-sur-Yvette
Mail: rachid.bennacer@ens-paris-saclay.fr

# STATEMENT

I declare that I am the co-author of the publication:

Coalescence of Sessile Aqueous Droplets Laden with Surfactant., Phys. Fluids, **36, (2024)**,https://doi.org/10. 1063/5. 0194816

My contributions included supporting conceptualization, participating in discussions, and reviewing/editing the draft.

signature:

Tianjin University

Zhizhao Che, PhD, Professor

State Key Laboratory of Engines, Tianjin University

135 Yaguan Road, Haihe Education Park,

Tianjin, 300350, China

Email: chezhizhao@tju.edu.cn

# STATEMENT

I declare that I am the co-author of the publication:

Coalescence of Sessile Aqueous Droplets Laden with Surfactant., Phys. Fluids, **36**, (2024),https://doi.org/10.1063/5.0194816

My contributions included supporting conceptualization, participating in discussions, and reviewing/editing the draft.

signature:

Dr hab. Panagiotis Theodorakis
Division of Theoretical Physics (ON5)
Al. Lotników 32/46
02-668 Warsaw, Poland

# STATEMENT

I declare that I am the co-author of the publication:

- **Coalescence of sessile aqueous droplets laden with surfactant**
  S. Arbabi, P. Deuar, R. Bennacer, Z. Che, P. E. Theodorakis
  *Phys. Fluids* **36**, … (2024), doi : 10.1063/5.0194816

My contribution was supervising the project, helping in the interpretation of the results, and in manuscript writing.

Warsaw, 06.02.2024
Panagiotis Theodorakis

## 4.4 Coalescence of Sessile Polymer Droplets: A Molecular Dynamics Study

### 4.4.1 Summary of Key Findings of this Publication:

In this paper, we investigate the coalescence of sessile polymer droplets on various substrates, encompassing both wettable and non-wettable surfaces. In this study, we used a physics-based CG force field for polymer chains where a standard bead–spring model has been employed. Our primary goal is to elucidate the role of viscosity, where longer polymer chain lengths correspond to higher viscosity, through the use of molecular dynamics simulations. These droplets are deposited onto substrates with different levels of wettability, a characteristic determined by the equilibrium contact angles of individual droplets, ranging from angles above to below 90 degrees (i.e. with angles ranging from 78° to 118°). The key findings of this work are summarized as follows:

- The dynamics of the bridge height are notably slower in the case of polymer droplets when compared to what is observed for our study on sessile water and surfactant-laden droplets [4]. Additionally, the coalescence process decelerates significantly as the polymer chain length increases. Similar to surfactant-laden droplets, we can observe the presence of an initial thermal regime followed by an inertial regime. This inertial regime exhibits growth based on a power law with an exponent lower than 0.5 for non-wettable substrate and lower than 2/3 for wettable substrate (contact angle less than 90°), which are reported in the case of coalescence of sessile water droplets. Furthermore, it is demonstrated that increasing the polymer chain length results in a gradual decrease of the exponent.
- We explored the dynamics of bridge shape by measuring a quantity named the bridge angle, $\theta$, (Fig. 1 in the paper). Overall, a steady decrease in the angle is observed across all polymer chain lengths. The decrease of the angle over time shows similar dynamics for polymer chain length over 80 beads. However, it decreases with a faster rate for the polymer chain length of 10 beads.
- The dynamics of coalescence were further explored by measuring the velocity of approach of two droplets on a substrate. For less wettable substrates, two different regimes with a noticeable transition between them were observed. This transition becomes more pronounced as the polymer chain length exceeds 40, and it appears smoother in the case of shorter chain lengths.

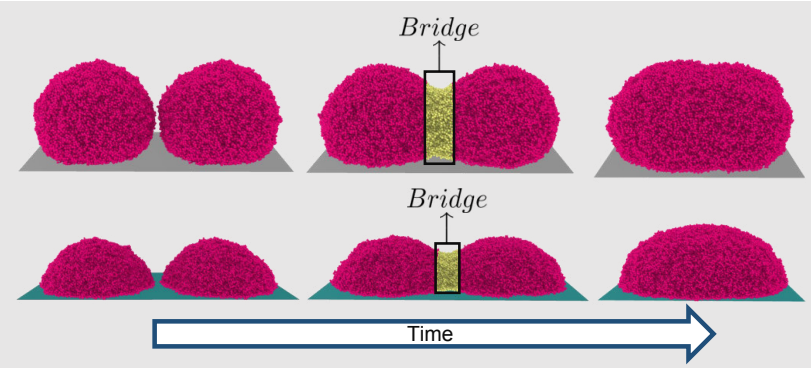


**Figure 4.4:** Coalescence of sessile polymer droplets. Reprinted from [Soheil Arbabi, Panagiotis E. Theodorakis, *Coalescence of Sessile Polymer Droplets: A Molecular Dynamics Study*, Macromol. Theory Simul. **32**, 2300017 (2023) https://doi.org/10.1002/mats.202300017, with permission of John Wiley and Sons, Inc.].

### 4.4.2 Details of Publication

**Coalescence of Sessile Polymer Droplets: A Molecular Dynamics Study**

PDF of this publication is reprinted from [Soheil Arbabi, Panagiotis E. Theodorakis, *Coalescence of Sessile Polymer Droplets: A Molecular Dynamics Study*, Macromol. Theory Simul. **32**, 2300017 (2023). https://doi.org/10.1002/mats.202300017, with permission of John Wiley and Sons, Inc.].

INSTYTUT FIZYKI
POLSKIEJ AKADEMII NAUK

Soheil Arbabi

Institute of Physics, Polish Academy of Sciences (PAN)

Theoretical Physics Division (ON5),

Al. Lotników 32/46 02-668 Warsaw, Poland

arbabi@ifpan.edu.pl

# STATEMENT

I declare that I am the co-author of the publication:

Coalescence of Sessile Polymer Droplets: A Molecular Dynamics Study.
Macromol. Theory Simul., **32**, 2300017 (2023).
https://doi.org/10.1002/mats.202300017

I contributed equally to the conceptualization. I took the lead role in data curation, analysis, investigation, methodology, simulations, validation, and visualization. In addition, I played an equal part in review, and editing tasks.

signature:
Soheil Arbabi

Dr hab. Panagiotis Theodorakis
Division of Theoretical Physics (ON5)
Al. Lotników 32/46
02-668 Warsaw, Poland

# STATEMENT

I declare that I am the co-author of the publication:

- **Coalescence of sessile polymer droplets: A molecular dynamics study**
  S. Arbabi, P. E. Theodorakis
  *Macromol. Theory Simul.* **32,** 2300017 (2023), doi : 10.1002/mats.202300017

My contribution was supervising the project, helping in the interpretation of the results, and in manuscript writing.

Warsaw, 09.12.2023
Panagiotis Theodorakis

# Chapter 5

# Conclusions and Outlook

This thesis has explored a broad spectrum of both macroscopic and microscopic characteristics during the coalescence of both freely suspended and sessile droplets. The primary focus has extended to surfactant-laden droplets with concentrations within the range relevant for applications and industrial use, typically exceeding the CAC. The thesis has demonstrated how surfactant mass transport and various geometrical features have operated during the process. This has included considerations of different types of surfactants, a range of concentration levels, and varying wettabilities, in the case of sessile droplets.

Considering the freely suspended droplets, this study has demonstrated that over a wide range of regimes the mass transport mechanism and flow patterns are generally unaffected by the type of surfactant used. It is observed that at higher concentrations (above CAC), water molecules do not participate in the initial stage of coalescence (pinching moment). The development of the initial pinching point, the process of bridge formation, and the creation of new aggregates within the bridge are investigated. When it comes to surfactant types, differences between Silewt-L77 and $C_iE_j$ surfactants have been discussed within the bridge growth process. Furthermore, this research has revealed the presence of an initial thermal regime, followed by an inertial regime. This inertial regime exhibits growth patterns based on a power-law with an exponent close to 0.5, which is in agreement with macroscopic theories [24, 64]. Bridge growth dynamics and in general coalescence process become slower as surfactant concentration grows.

In the examination of coalescence in sessile surfactant-laden droplets on different substrates with varying wettabilities, it is demonstrated that, for non-wettable substrates ($\theta_s > 90^\circ$), the mass transport mechanism and bridge growth dynamics closely resemble those of freely suspended droplets. The process initiates far from the substrate, and after an initial thermal regime, it undergoes an inertial regime characterized by a power-law with an exponent of around 0.5. On the other hand, droplets on more wettable substrates ($\theta_s > 90^\circ$) exhibit distinct behavior. In this case, the bridge grows on the substrate, and after the initial thermal regime, it follows a power-law with an exponent close to $2/3$. Coalescence begins with hydrophobic beads; however, a more significant involvement of water is observed on wettable substrates compared

to non-wettable substrates. One notable finding of this research is the absence of new aggregates inside the bridge bulk in the case of a wettable substrate ($\theta_s \simeq 50^\circ$).

To assess the impact of viscosity and substrate on coalescence, further study is conducted on the dynamics of coalescence of sessile polymer droplets with varying chain lengths. These droplets were placed on substrates with different levels of wettability, encompassing contact angles both below and above $90^\circ$. In general, polymer droplets exhibited slower rates of bridge development and coalescence compared to water and surfactant-laden droplets. Furthermore, an observed decrease in the speed of coalescence and bridge dynamics is correlated with the increased length of polymer chains. Moreover, the velocity of approach of polymer droplets by measuring the distance between center of masses of two droplets are further analyzed. In the case of a non-wettable substrate ($\theta_s > 90^\circ$), two distinct regimes are observed with a noticeable transition between them, this transition becomes more pronounced for droplets with longer polymer chain lengths. On the other hand, for wettable substrates ($\theta_s < 90^\circ$), the distance between droplets smoothly decreases within a single linear regime. Based on our studies, a possible extension might include the investigation of droplet coalescence under confinement, such as micro/nano-channels of varying wettability, where surfactant molecules are also present. For example, in bio-related studies and microfluidics, bio-particles are encapsulated within droplets, and the addition of surfactant can play a role in impeding the coalescence process.

# Bibliography


[1] D. G. Aarts, H. N. Lekkerkerker, H. Guo, G. H. Wegdam, and D. Bonn. "Hydrodynamics of droplet coalescence". In: *Phys. Rev. Lett.* 95.16 (2005), p. 164503. DOI: 10.1103/PhysRevLett.95.164503.

[2] A. Aasen, M. Hammer, Å. Ervik, E. A. Müller, and Ø. Wilhelmsen. "Equation of state and force fields for Feynman–Hibbs-corrected Mie fluids. I. Application to pure helium, neon, hydrogen, and deuterium". In: *J. Chem. Phys.* 151.6 (2019). DOI: 10.1063/1.5111364.

[3] D. Anghel, S. Saito, A. Băran, A. Iovescu, and M. Corniţescu. "The aggregation of nonionic surfactants in the presence of poly (methacrylic acid)". In: *Colloid and Polymer Science* 285 (2007), pp. 771–779. DOI: 10.1007/s00396-006-1617-1.

[4] S. Arbabi, P. Deuar, R. Bennacer, Z. Che, and P. E. Theodorakis. "Coalescence of Sessile Aqueous Droplets Laden with Surfactant". In: *Phys. Fluids* 36 (2024). DOI: 10.1063/5.0194816.

[5] S. Arbabi, P. Deuar, M. Denys, R. Bennacer, Z. Che, and P. E. Theodorakis. "Coalescence of surfactant-laden droplets". In: *Phys. Fluids* 35 (2023), p. 063329. DOI: 10.1063/5.0153676.

[6] S. Arbabi, P. Deuar, M. Denys, R. Bennacer, Z. Che, and P. E. Theodorakis. "Molecular dynamics simulation of the coalescence of surfactant-laden droplets". In: *Soft Matter* 19.42 (2023), pp. 8070–8080. DOI: 10.1039/D3SM01046E.

[7] S. Arbabi and P. E. Theodorakis. "Coalescence of Sessile Polymer Droplets: A Molecular Dynamics Study". In: *Macromol. Theory Simul.* n/a.n/a (2023), p. 2300017. DOI: 10.1002/mats.202300017.

[8] N. Ashgriz and J. Poo. "Coalescence and separation in binary collisions of liquid drops". In: *J. Fluid Mech.* 221 (1990), pp. 183–204. DOI: 10.1017/S0022112090003536.

[9] C. Avendaño, T. Lafitte, A. Galindo, C. S. Adjiman, G. Jackson, and E. A. Müller. "SAFT-$\gamma$ Force Field for the Simulation of Molecular Fluids. 1. A Single-Site Coarse Grained Model of Carbon Dioxide". In: *J. Phys. Chem B* 115 (2011), pp. 11154–11169. DOI: 10.1021/jp204908d.

[10] C. Avendaño, T. Lafitte, A. Galindo, C. S. Adjiman, E. A. Müller, and G. Jackson. "SAFT-$\gamma$ Force Field for the Simulation of Molecular Fluids: 2. Coarse-Grained Models of Greenhouse Gases". In: *J. Phys. Chem B* 117 (2013), pp. 2717–2733. DOI: 10.1021/jp306442b.

[11] P. Banerjee, S. Roy, and N. Nair. "Coarse-grained molecular dynamics force-field for polyacrylamide in infinite dilution derived from iterative Boltzmann inversion and MARTINI force-field". In: *J. Phys. Chem. B.* 122.4 (2018), pp. 1516–1524. DOI: 10.1021/acs.jpcb.7b09019.

[12] J.-C. Baret. "Surfactants in droplet-based microfluidics". In: *Lab Chip* 12.3 (2012), pp. 422–433. DOI: 10.1039/C1LC20582J.

[13] V. Boţan, V. D. Ustach, K. Leonhard, and R. Faller. "Development and application of a coarse-grained model for PNIPAM by iterative Boltzmann inversion and its combination with lattice Boltzmann hydrodynamics". In: *J. Phys. Chem. B.* 121.45 (2017), pp. 10394–10406. DOI: 10.1021/acs.jpcb.7b07818.

[14] E. G. Bowen. "The formation of rain by coalescence". In: *Aust. J. Chem.* 3.2 (1950), pp. 193–213. DOI: 10.1071/CH9500193.

[15] B. R. Brooks, C. L. Brooks III, A. D. Mackerell Jr, L. Nilsson, R. J. Petrella, B. Roux, Y. Won, G. Archontis, C. Bartels, S. Boresch, et al. "CHARMM: the biomolecular simulation program". In: *J. Comput. Chem.* 30.10 (2009), pp. 1545–1614. DOI: 10.1002%2Fjcc.21287.

[16] J. Burton and P. Taborek. "Role of dimensionality and axisymmetry in fluid pinch-off and coalescence". In: *Phys. Rev. Lett.* 98.22 (2007), p. 224502. DOI: 10.1103/PhysRevLett.98.224502.

[17] W. G. Chapman, K. E. Gubbins, G. Jackson, and M. Radosz. "SAFT: Equation-of-state solution model for associating fluids". In: *Fluid Phase Equil.* 52 (1989), pp. 31–38. DOI: 10.1016/0378-3812(89)80308-5.

[18] A. J. Cohen, P. Mori-Sánchez, and W. Yang. "Challenges for density functional theory". In: *Chem. Rev.* 112.1 (2012), pp. 289–320. DOI: 10.1021/cr200107z.

[19] M. Denys, P. Deuar, Z. Che, and P. E. Theodorakis. "A Lagrangian particle-based numerical model for surfactant-laden droplets at macroscales". In: *Phys. Fluids* 34.9 (2022), p. 095126. DOI: 10.1063/5.0101930.

[20] C. J. Dickson, B. D. Madej, Å. A. Skjevik, R. M. Betz, K. Teigen, I. R. Gould, and R. C. Walker. "Lipid14: the amber lipid force field". In: *J. Chem. Theory Comput.* 10.2 (2014), pp. 865–879. DOI: 10.1021/ct4010307.

[21] L. Duchemin, J. Eggers, and C. Josserand. "Inviscid coalescence of drops". In: *J. Fluid Mech.* 487 (2003), pp. 167–178. DOI: 10.1017/S0022112003004646.

[22] M. Dudek, J. Chicault, and G. Øye. "Microfluidic investigation of crude oil droplet coalescence: effect of oil/water composition and droplet aging". In: *Energy Fuels* 34.5 (2019), pp. 5110–5120. DOI: 10.1021/acs.energyfuels.9b03434.

[23] A. Eddi, K. Winkels, and J. Snoeijer. "Influence of droplet geometry on the coalescence of low viscosity drops". In: *PRL* 111.14 (2013), p. 144502. DOI: 10.1103/PhysRevLett.111.144502.

[24] J. Eggers, J. R. Lister, and H. A. Stone. "Coalescence of liquid drops". In: *J. Fluid Mech.* 401 (1999), pp. 293–310. DOI: 10.1017/S002211209900662X.

[25] M. Fayaz-Torshizi and E. A. Müller. "Coarse-Grained Molecular Simulation of Polymers Supported by the Use of the SAFT-$\gamma$ $\gamma$ Mie Equation of State". In: *Macromol Theory Simul* 31.1 (2022), p. 2100031. DOI: 10.1002/mats.202100031.

[26] S. Feng, L. Yi, L. Zhao-Miao, C. Ren-Tuo, and W. Gui-Ren. "Advances in micro-droplets coalescence using microfluidics". In: *Chin J Anal Chem*, 43.12 (2015), pp. 1942–1954. DOI: 10.1016/S1872-2040(15)60886-6.

[27] A. Gautieri, A. Russo, S. Vesentini, A. Redaelli, and M. J. Buehler. "Coarse-grained model of collagen molecules using an extended MARTINI force field". In: *J. Chem. Theory Comput.* 6.4 (2010), pp. 1210–1218. DOI: 10.1021/ct100015v.

[28] M. Gross, I. Steinbach, D. Raabe, and F. Varnik. "Viscous coalescence of droplets: A lattice Boltzmann study". In: *Phys. Fluids* 25.5 (2013), p. 052101. DOI: 10.1063/1.4803178.

[29] M. A. Hack, P. Vondeling, M. Cornelissen, D. Lohse, J. H. Snoeijer, C. Diddens, and T. Segers. "Asymmetric coalescence of two droplets with different surface tensions is caused by capillary waves". In: *Phys. Rev. Fluids* 6.10 (2021), p. 104002. DOI: 10.1103/PhysRevFluids.6.104002.

[30] E. Harder, W. Damm, J. Maple, C. Wu, M. Reboul, J. Y. Xiang, L. Wang, D. Lupyan, M. K. Dahlgren, J. L. Knight, et al. "OPLS3: a force field providing broad coverage of drug-like small molecules and proteins". In: *J. Chem. Theory Comput.* 12.1 (2016), pp. 281–296. DOI: 10.1021/acs.jctc.5b00864.

[31] C. Herdes Moreno, A. Ervik, A. Mejia, and E. Muller. "Prediction of the water/oil interfacial tension from molecular simulations using the coarse-grained SAFT-$\gamma$ Mie force field". In: *Fluid Phase Equilibria* 476 (2018), pp. 9–15. DOI: 10.1016/j.fluid.2017.06.016.

[32] R. W. Hopper. "Plane Stokes flow driven by capillarity on a free surface". In: *J. Fluid Mech.* 213 (1990), pp. 349–375. DOI: 10.1017/S002211209000235X.

[33] N. Jaensson and J. Vermant. "Tensiometry and rheology of complex interfaces". In: *Curr. Opin. Colloid Interface Sci.* 37 (2018), pp. 136–150. DOI: 10.1016/j.cocis.2018.09.005.

[34] Y. Jiang, A. Umemura, and C. K. Law. "An experimental investigation on the collision behaviour of hydrocarbon droplets". In: *J. Fluid Mech.* 234 (1992), pp. 171–190. DOI: 10.1017/S0022112092000740.

[35] J. Jin, C. H. Ooi, D. V. Dao, and N.-T. Nguyen. "Coalescence processes of droplets and liquid marbles". In: *Micromachines* 8.11 (2017), p. 336. DOI: 10.3390/mi8110336.

[36] J. E. Jones. "On the determination of molecular fields.—I. From the variation of the viscosity of a gas with temperature". In: *Proceedings of the Royal Society of London. Series A, Containing Papers of a Mathematical and Physical Character* 106.738 (1924), pp. 441–462. DOI: 10.1098/rspa.1924.0082.

[37] D. H. de Jong, G. Singh, W. F. D. Bennett, C. Arnarez, T. A. Wassenaar, L. V. Schäfer, X. Periole, D. P. Tieleman, and S. J. Marrink. "Improved Parameters for the Martini Coarse-Grained Protein Force Field". In: *J. Chem. Theory Comput.* 9.1 (2013), pp. 687–697. DOI: 10.1021/ct300646g.

[38] S. Kawamoto, H. Liu, Y. Miyazaki, S. Seo, M. Dixit, R. DeVane, C. MacDermaid, G. Fiorin, M. L. Klein, and W. Shinoda. "SPICA force field for proteins and peptides". In: *J. Chem. Theory Comput.* 18.5 (2022), pp. 3204–3217.

[39] M. I. Khodabocus, M. Sellier, and V. Nock. "Scaling Laws of Droplet Coalescence: Theory and Numerical Simulation". In: *Adv. Math. Phys.* 2018 (2018). DOI: 10.1155/2018/4906016.

[40] N. M. Kovalchuk, M. Reichow, T. Frommweiler, D. Vigolo, and M. J. H. Simmons. "Mass Transfer Accompanying Coalescence of Surfactant-Laden and Surfactant-Free Drop in a Microfluidic Channel". In: *Langmuir* 35.28 (2019), pp. 9184–9193. DOI: 10.1021/acs.langmuir.9b00843.

[41] T. Lafitte, A. Apostolakou, C. Avendaño, A. Galindo, C. S. Adjiman, E. A. Müller, and G. Jackson. "Accurate statistical associating fluid theory for chain molecules formed from Mie segments". In: *J. Chem. Phys.* 139 (2013), p. 154504. DOI: 10.1063/1.4819786.

[42] L. Leal. "Flow induced coalescence of drops in a viscous fluid". In: *Phys. Fluids* 16.6 (2004), pp. 1833–1851. DOI: 10.1063/1.1701892.

[43] Y.-C. Lee, H.-S. Liu, S.-Y. Lin, H.-F. Huang, Y.-Y. Wang, and L.-W. Chou. "An observation of the coexistence of multimers and micelles in a nonionic surfactant C10E4 solution by dynamic light scattering". In: *Journal of the Chinese Institute of Chemical Engineers* 39.1 (2008), pp. 75–83. DOI: 10.1016/j.jcice.2007.11.009.

[44] H. Lee, A. H. de Vries, S.-J. Marrink, and R. W. Pastor. "A Coarse-Grained Model for Polyethylene Oxide and Polyethylene Glycol: Conformation and Hydrodynamics". In: *J. Phys. Chem. B* 113.40 (2009), pp. 13186–13194. DOI: 10.1021/jp9058966.

[45] M. W. Lee, D. K. Kang, S. S. Yoon, and A. L. Yarin. "Coalescence of two drops on partially wettable substrates". In: *Langmuir* 28.8 (2012), pp. 3791–3798. DOI: 10.1021/la204867c.

[46] J. E. Lennard-Jones. "Cohesion". In: *Proc. Phys. Soc.* 43.5 (1931), p. 461.

[47] O. Lobanova, C. Avendaño, T. Lafitte, E. A. Müller, and G. Jackson. "SAFT-fl force field for the simulation of molecular fluids. 4. A single-site coarse-grained model of water applicable over a wide temperature range." In: *Mol. Phys.* 113 (2015), pp. 1228–1249. DOI: 10.1080/00268976.2015.1004804.

[48] O. Lobanova. "Development of coarse-grained force fields from a molecular based equation of state for thermodynamic and structural properties of complex fluids". PhD thesis. Imperial College London, 2014.

[49] C. A. López, Z. Sovova, F. J. van Eerden, A. H. de Vries, and S. J. Marrink. "Martini Force Field Parameters for Glycolipids". In: *J. Chem. Theory Comput.* 9.3 (2013), pp. 1694–1708. DOI: 10.1021/ct3009655.

[50] S. J. Marrink, A. H. De Vries, and A. E. Mark. "Coarse grained model for semi-quantitative lipid simulations". In: *J. Phys. Chem. B* 108.2 (2004), pp. 750–760. DOI: 10.1021/jp036508g.

[51] S. J. Marrink, H. J. Risselada, S. Yefimov, D. P. Tieleman, and A. H. De Vries. "The MARTINI force field: coarse grained model for biomolecular simulations". In: *J. Phys. Chem. B* 111.27 (2007), pp. 7812–7824. DOI: 10.1021/jp071097f.

[52] S. J. Marrink and D. P. Tieleman. "Perspective on the Martini model". In: *Chem Soc Rev* 42.16 (2013), pp. 6801–6822. DOI: 10.1039/C3CS60093A.

[53] L. Monticelli, S. K. Kandasamy, X. Periole, R. G. Larson, D. P. Tieleman, and S.-J. Marrink. "The MARTINI Coarse-Grained Force Field: Extension to Proteins". In: *J. Chem. Theory Comput.* 4.5 (2008), pp. 819–834. DOI: 10.1021/ct700324x.

[54] T. C. Moore, C. R. Iacovella, and C. McCabe. "Derivation of coarse-grained potentials via multistate iterative Boltzmann inversion". In: *Chem. Phys.* 140.22 (2014). DOI: doi.org/10.1063/1.4880555.

[55] E. A. Müller and G. Jackson. "Force field parameters from the SAFT-$\gamma$ equation of state for use in coarse-grained molecular simulations". In: *Annu. Rev. Chem. Biomol. Eng.* 5 (2014), pp. 405–427. DOI: 10.1146/annurev-chembioeng-061312-103314.

[56] E. A. Müller and K. E. Gubbins. "Molecular-based equations of state for associating fluids: A review of SAFT and related approaches". In: *Industrial & engineering chemistry research* 40.10 (2001), pp. 2193–2211.

[57] E. A. Müller and G. Jackson. "Force-field parameters from the SAFT-$\gamma$ equation of state for use in coarse-grained molecular simulations". In: *Annu. Rev. Chem. Biomol. Eng.* 5 (2014), pp. 405–427. DOI: 10.1146/annurev-chembioeng-061312-103314.

[58] E. A. Müller and K. E. Gubbins. "Molecular-Based Equations of State for Associating Fluids: A Review of SAFT and Related Approaches". In: *Industrial & Engineering Chemistry Research* 40.10 (2001), pp. 2193–2211. DOI: 10.1021/ie000773w.

[59] R. Narhe, D. Beysens, and Y. Pomeau. "Dynamic drying in the early-stage coalescence of droplets sitting on a plate". In: *EPL* 81.4 (2008), p. 46002. DOI: 10.1209/0295-5075/81/46002.

[60] E. Nowak, N. M. Kovalchuk, Z. Che, and M. J. Simmons. "Effect of surfactant concentration and viscosity of outer phase during the coalescence of a surfactant-laden drop with a surfactant-free drop". In: *Colloids Surf. A Physicochem. Eng. Asp.* 505 (2016), pp. 124–131. DOI: 10.1016/j.colsurfa.2016.02.016.

[61] E. Nowak, Z. Xie, N. M. Kovalchuk, O. K. Matar, and M. J. Simmons. "Bulk advection and interfacial flows in the binary coalescence of surfactant-laden and surfactant-free drops". In: *Soft Matter* 13.26 (2017), pp. 4616–4628. DOI: 10.1039/C7SM00328E.

[62] N. Pallas and Y. Harrison. "An automated drop shape apparatus and the surface tension of pure water". In: *Colloids Surf.* 43.2 (1990), pp. 169–194. DOI: 10.1016/0166-6622(90)80287-E.

[63] J. D. Paulsen, R. Carmigniani, A. Kannan, J. C. Burton, and S. R. Nagel. "Coalescence of bubbles and drops in an outer fluid". In: *Nat. Commun.* 5 (2014), p. 3182. DOI: 10.1038/ncomms4182.

[64] J. D. Paulsen. "Approach and coalescence of liquid drops in air". In: *Phys. Rev. E* 88.6 (2013), p. 063010. DOI: 10.1103/PhysRevE.88.063010.

[65] J. D. Paulsen, J. C. Burton, S. R. Nagel, S. Appathurai, M. T. Harris, and O. A. Basaran. "The inexorable resistance of inertia determines the initial regime of drop coalescence". In: *Proc. Natl. Acad. Sci. U.S.A.* 109.18 (2012), pp. 6857–6861. DOI: 10.1073/pnas.1120775109.

[66] J. D. Paulsen, J. C. Burton, and S. R. Nagel. "Viscous to Inertial Crossover in Liquid Drop Coalescence". In: *Phys. Rev. Lett.* 106 (11 2011), p. 114501. DOI: 10.1103/PhysRevLett.106.114501.

[67] X. Periole, M. Cavalli, S.-J. Marrink, and M. A. Ceruso. "Combining an Elastic Network With a Coarse-Grained Molecular Force Field: Structure, Dynamics, and Intermolecular Recognition". In: *J. Chem. Theory Comput.* 5.9 (2009), pp. 2531–2543. DOI: 10.1021/ct9002114.

[68] S. Perumanath, M. K. Borg, M. V. Chubynsky, J. E. Sprittles, and J. M. Reese. "Droplet coalescence is initiated by thermal motion". In: *Phys. Rev. Lett.* 122.10 (2019), p. 104501. DOI: 10.1103/PhysRevLett.122.104501.

[69] J. J. Potoff and D. A. Bernard-Brunel. "Mie potentials for phase equilibria calculations: Application to alkanes and perfluoroalkanes". In: *J. Phys. Chem. B* 113.44 (2009), pp. 14725–14731. DOI: 10.1021/jp9072137.

[70] T. D. Potter, J. Tasche, E. L. Barrett, M. Walker, and M. R. Wilson. "Development of new coarse-grained models for chromonic liquid crystals: insights from top-down approaches". In: *Liq. Cryst.* 44.12-13 (2017), pp. 1979–1989. DOI: 10.1080/02678292.2017.1342005.

[71] J. Qian and C. K. Law. "Regimes of coalescence and separation in droplet collision". In: *J. Fluid Mech.* 331 (1997), pp. 59–80. DOI: 10.1017/S0022112096003722.

[72] M. M. Reif, M. Winger, and C. Oostenbrink. "Testing of the GROMOS force-field parameter set 54A8: structural properties of electrolyte solutions, lipid bilayers, and proteins". In: *J. Chem. Theory Comput.* 9.2 (2013), pp. 1247–1264. DOI: 10.1021/ct300874c.

[73] W. Ristenpart, P. McCalla, R. Roy, and H. Stone. "Coalescence of spreading droplets on a wettable substrate". In: *Phys. Rev. Lett.* 97.6 (2006), p. 064501. DOI: 10.1103/PhysRevLett.97.064501.

[74] G. Rossi, L. Monticelli, S. R. Puisto, I. Vattulainen, and T. Ala-Nissila. "Coarse-graining polymers with the MARTINI force-field: polystyrene as a benchmark case". In: *Soft Matter* 7.2 (2011), pp. 698–708. DOI: 10.1039/C0SM00481B.

[75] V. Ruhle, C. Junghans, A. Lukyanov, K. Kremer, and D. Andrienko. "Versatile object-oriented toolkit for coarse-graining applications". In: *J. Chem. Theory Comput.* 5.12 (2009), pp. 3211–3223. DOI: 10.1021/ct900369w.

[76] E. E. Santiso, C. Herdes, and E. A. Müller. "On the calculation of solid-fluid contact angles from molecular dynamics". In: *Entropy* 15.9 (2013), pp. 3734–3745. DOI: 10.3390/e15093734.

[77] M. G. Saunders and G. A. Voth. "Coarse-graining methods for computational biology". In: *Annu. Rev. Biophys.* 42 (2013), pp. 73–93. DOI: 10.1146/annurev-biophys-083012-130348.

[78] S. Seo and W. Shinoda. "SPICA force field for lipid membranes: domain formation induced by cholesterol". In: *J. Chem. Theory Comput.* 15.1 (2018), pp. 762–774. DOI: 10.1021/acs.jctc.8b00987.

[79] W. Shinoda, R. DeVane, and M. L. Klein. "Coarse-grained molecular modeling of non-ionic surfactant self-assembly". In: *Soft Matter* 4.12 (2008), pp. 2454–2462. DOI: 10.1039/B808701F.

[80] V. S. Sivasankar, S. A. Etha, D. R. Hines, and S. Das. "Coalescence of Microscopic Polymeric Drops: Effect of Drop Impact Velocities". In: *Langmuir* 37.45 (2021), pp. 13512–13526. DOI: 10.1021/acs.langmuir.1c02337.

[81] V. S. Sivasankar, D. R. Hines, and S. Das. "Numerical Study of the Coalescence and Mixing of Drops of Different Polymeric Materials". In: *Langmuir* 38.46 (2022), pp. 14084–14096. DOI: 10.1021/acs.langmuir.2c02029.

[82] E. R. Smith and P. E. Theodorakis. "Multiscale simulation of fluids: coupling molecular and continuum". In: *Phys. Chem. Chem. Phys.* 26 (2 2024), pp. 724–744. DOI: 10.1039/D3CP03579D.

[83] P. C. T. Souza, R. Alessandri, J. Barnoud, S. Thallmair, I. Faustino, F. Grünewald, I. Patmanidis, H. Abdizadeh, B. M. H. Bruininks, T. A. Wassenaar, P. C. Kroon, J. Melcr, V. Nieto, V. Corradi, H. M. Khan, J. Domański, M. Javanainen, H. Martinez-Seara, N. Reuter, R. B. Best, I. Vattulainen, L. Monticelli, X. Periole, D. P. Tieleman, A. H. de Vries, and S. J. Marrink. "Martini 3: a general purpose force field for coarse-grained molecular dynamics". In: *Nat. Methods* 18 (2021), pp. 382–388. DOI: 10.1038/s41592-021-01098-3.

[84] J. Sprittles and Y. Shikhmurzaev. "Coalescence of liquid drops: Different models versus experiment". In: *Phys. Fluids* 24.12 (2012), p. 122105. DOI: 10.1063/1.4773067.

[85] S. Stephan and U. K. Deiters. "Characteristic curves of the Lennard-Jones fluid". In: *Int. J. Thermophys.* 41 (2020), pp. 1–24. DOI: 10.1007/s10765-020-02721-9.

[86] A. Stukowski. "Visualization and analysis of atomistic simulation data with OVITO–the Open Visualization Tool". In: *Modelling Simul. Mater. Sci. Eng.* 18 (2010), p. 015012. DOI: 10.1088/0965-0393/18/1/015012.

[87] P. E. Theodorakis, E. A. Müller, R. V. Craster, and O. K. Matar. "Modelling the superspreading of surfactant-laden droplets with computer simulation". In: *Soft Matter* 11.48 (2015), pp. 9254–9261. DOI: 10.1039/C5SM02090E.

[88] P. E. Theodorakis, E. A. Müller, R. V. Craster, and O. K. Matar. "Superspreading: Mechanisms and Molecular Design". In: *Langmuir* 31.8 (2015), pp. 2304–2309. DOI: 10.1021/la5044798.

[89] T. Thomas and H. N. Unni. "LED-based opto-wetting and fluidic transport for droplet mixing". In: *Microfluid Nanofluidics* 23 (2019), pp. 1–12. DOI: 10.1007%2Fs10404-019-2273-3.

[90] S. Thoroddsen, K. Takehara, and T. Etoh. "The coalescence speed of a pendent and a sessile drop". In: *J. Fluid Mech.* 527 (2005), pp. 85–114. DOI: 10.1017/S0022112004003076.

[91] J. J. Uusitalo, H. I. Ingólfsson, P. Akhshi, D. P. Tieleman, and S. J. Marrink. "Martini Coarse-Grained Force Field: Extension to DNA". In: *J. Chem. Theory Comput.* 11.8 (2015), pp. 3932–3945. DOI: 10.1021/acs.jctc.5b00286.

[92] P. Vainikka, S. Thallmair, P. C. T. Souza, and S. J. Marrink. "Martini 3 Coarse-Grained Model for Type III Deep Eutectic Solvents: Thermodynamic, Structural, and Extraction Properties". In: *ACS Sustain. Chem. Eng.* 9.51 (2021), pp. 17338–17350. DOI: 10.1021/acssuschemeng.1c06521.

[93] J. Wohlert and L. A. Berglund. "A coarse-grained model for molecular dynamics simulations of native cellulose". In: *J. Chem. Theory Comput.* 7.3 (2011), pp. 753–760. DOI: 10.1021/ct100489z.

[94] X. Xia, C. He, and P. Zhang. "Universality in the viscous-to-inertial coalescence of liquid droplets". In: *Proceedings of the National Academy of Sciences* 116.47 (2019), pp. 23467–23472. DOI: 10.1073/pnas.1910711116.

[95] H. O. Yadav, S. Harada, A.-T. Kuo, S. Urata, and W. Shinoda. "Hemimicelle formation of semi-fluorocarbon chains at air–water interface: coarse-grained molecular dynamics study with an extension of the SPICA force field". In: *Mol. Phys.* 119.19-20 (2021), e1910355. DOI: 10.1080/00268976.2021.1910355.

[96] S. O. Yesylevskyy, L. V. Schäfer, D. Sengupta, and S. J. Marrink. "Polarizable Water Model for the Coarse-Grained MARTINI Force Field". In: *PLOS Comput. Biol.* 6.6 (June 2010), pp. 1–17. DOI: 10.1371/journal.pcbi.1000810.

[97] Y. Yoon, F. Baldessari, H. D. Ceniceros, and L. G. Leal. "Coalescence of two equal-sized deformable drops in an axisymmetric flow". In: *Phys. Fluids* 19.10 (2007), p. 102102. DOI: 10.1063/1.2772900.

Dostępy do artykułów:

**Soheil Arbabi**, Piotr Deuar, Mateusz Denys, Rachid Bennacer, Zhizhao Che, Panagiotis E. Theodorakis; Coalescence of surfactant-laden droplets. ***Phys. Fluids*** **35** 063329 (2023). https://doi.org/10.1063/5.0153676

**Soheil Arbabi**, Piotr Deuar, Mateusz Denys, Rachid Bennacer, Zhizhao Che, and Panagiotis E. Theodorakis. "Molecular dynamics simulation of the coalescence of surfactant-laden droplets." ***Soft Matter*** **19**, 8070-8080 (2023). https://doi.org/10.1039/D3SM01046E

**Soheil Arbabi**, Piotr Deuar, Rachid Bennacer, Zhizhao Che, and Panagiotis E. Theodorakis, Coalescence of Sessile Aqueous Droplets Laden with Surfactant. ***Phys. Fluids*** **36**, XXXXX (2024). https://doi.org/10.1063/5.0194816

**Soheil Arbabi**, Panagiotis E. Theodorakis, Coalescence of Sessile Polymer Droplets: A Molecular Dynamics Study. ***Macromol. Theory Simul.*** **32**, 2300017 (2023). https://doi.org/10.1002/mats.202300017